Available online at www.sciencedirect.com
ScienceDirect
Journal of Catalysis 247 (2007) 176–193
JOURNAL OF CATALYSIS
www.elsevier.com/locate/jcat

Active species on γ-alumina-supported vanadia catalysts: Nature and reducibility

Frank Klose [a,b], Tania Wolff [a], Heike Lorenz [a], Andreas Seidel-Morgenstern [a,c], Yuri Suchorski [d], Monika Piórkowska [d], Helmut Weiss [d,*]

[a] *Max-Planck-Institut für Dynamik Komplexer Technischer Systeme, Sandtorstraße 1, D-39106 Magdeburg, Germany*
[b] *Otto-von-Guericke-Universität Magdeburg, Institut für Automatisierungstechnik, Universitätsplatz 2, D-39106 Magdeburg, Germany*
[c] *Otto-von-Guericke-Universität Magdeburg, Institut für Verfahrenstechnik, Universitätsplatz 2, D-39106 Magdeburg, Germany*
[d] *Otto-von-Guericke-Universität Magdeburg, Chemisches Institut, Universitätsplatz 2, D-39106 Magdeburg, Germany*

Received 3 July 2006; revised 22 January 2007; accepted 23 January 2007

Available online 7 March 2007

Abstract

The oxidation states and reducibility of γ-alumina-supported vanadium oxide catalysts with V loadings between 1.7 and 15.7 wt% were studied by means of temperature-programmed reduction (TPR) and X-ray photoelectron spectroscopy (XPS) for fresh as well as used catalysts. As additional experimental techniques, X-ray diffraction (XRD), diffuse reflectance infrared Fourier-transform spectroscopy (DRIFTS), and temperature-programmed desorption (TPD) were applied. For V loadings up to 6.1 wt%, the surface was found to be covered only by vanadate, while at higher loadings the formation of V_2O_5 crystallites was observed. The XPS and TPR data showed that under moderate oxidizing conditions, only ∼30% of V in the vanadate catalysts was in the oxidation state +5, while in the catalysts containing V_2O_5 crystallites it was about 80%, with the remainder being present as V(IV) in both cases. In the ambient pressure TPR experiments, all catalysts were completely reduced by hydrogen to V(III), although the vanadate catalysts were found to be more easily reducible than those containing V_2O_5. The V dispersion changed during redox cycles, as they appeared under working conditions. These changes were different for the exposure to ethane or hydrogen, but did not influence the maximum oxidation states. In the catalytic oxidation of ethane used as a model reaction, all catalysts were found to be in their oxidized state under steady-state conditions. Significant catalyst reduction occurred only if the surrounding gas-phase oxygen was completely consumed, leading to the loss of catalytic activity due to the disappearance of V(V) species. A novel structure for γ-alumina-supported vanadia catalysts is proposed on the basis of the experimental data.

Keywords: Supported vanadia catalysts; Vanadia phases; Reducibility, Ethane oxidation; Selective oxidation, XPS; TPR; XRD; DRIFTS; TPD

1. Introduction

Supported vanadium oxide catalysts are known to be active in the selective oxidation and ammoxidation of hydrocarbons and other organic substrates [1,2]. Commercial large-scale processes were developed for the oxidation of methanol to formaldehyde, the oxidation of *o*-xylene to phthalic anhydride, the ammoxidation of aromatic hydrocarbons, the oxidation of sulphur dioxide to sulphur trioxide, for selective catalytic reduction (SCR) in waste gas treatment (see, e.g., [3,4]), and other uses. In addition, much effort has been spent over the last decades to develop suitable vanadium oxide-based catalysts for the oxidative dehydrogenation and selective oxidation of light hydrocarbons to valuable olefins and oxygenates, but these processes are still far from industrial application [3]. Due to the huge importance of vanadium oxide catalysts in oxidation reactions, it is of great interest to improve our understanding of the nature of the active species and their role under reaction conditions.

In the selective oxidation of hydrocarbons, vanadia is typically deposited onto high-area support materials such as γ-alumina, silica, titania, or zirconia to increase the number of active sites and obtain better catalytic activity. During catalyst calci-

* Corresponding author. Fax: +49 0 391 6711387.
E-mail address: helmut.weiss@vst.uni-magdeburg.de (H. Weiss).

0021-9517/$ – see front matter
doi:10.1016/j.jcat.2007.01.013

nation, the vanadium oxide formed intermediately by precursor oxidation undergoes a chemical interaction with the support, resulting in the formation of M–O–V bonds (M is the cation of the support material). The strength of the support–vanadia interaction is strongly dependent on the coverage and the nature of the support, leading at low coverage to formation of thin vanadate layers and at higher loadings and weak support–vanadia interaction to agglomeration of bulk-like V_2O_5 crystallites [5–9]. For the partial oxidation of hydrocarbons, vanadate species are found to be more active and selective than bulk-phase V_2O_5; thus, formation of the latter should be suppressed. Furthermore, the M–O–V bonds are assumed to be crucial to the reducibility and acid–base properties of the catalysts, which are important for both activity and selectivity as well.

Regarding the chemical nature of vanadate species, the existence of monovanadate and polyvanadate is suggested (see, e.g. [10–14]). Monovanadates, as the most dispersed V species, are assumed to appear predominantly at low V loadings. Their base VO_4 unit consists of one V=O double bond and three M–O–V bonds to the support. Polyvanadate species formed at moderately higher V loadings on some, but not all supports (e.g., not on silica) also contain V–O–V bonds [15]. These vanadate species form a two-dimensional network until the surface of the support is completely covered (so-called monolayer coverage). Only if this monolayer coverage is exceeded does formation of three-dimensional $(V_2O_5)_n$ crystallites occur, and the V dispersion decreases rapidly. The monolayer coverage, which can be calculated as a theoretical value from the geometry of the different vanadate species [16], is commonly given with 2.3 V atoms/nm^2 for monovanadates and 7 V atoms/nm^2 for polyvanadates [17–19].

In practice, the dispersion of vanadia on various supports depends strongly on the nature of the latter as well as on the method of catalyst preparation, leading to different maximum possible V densities before the formation of crystallized V_2O_5 occurs [10,14]. Weckhuysen and Keller [14], summarizing a large number of studies, gave values of around 5–10 V/nm^2 for γ-Al_2O_3, TiO_2, and ZrO_2 but only $\sim$1 V/nm^2 for SiO_2. Blasco and Nieto [20] related the tendency of V_2O_5 agglomeration to the acid–base character of the support. Basic supports yield higher vanadia dispersion due to a stronger reaction with the acidic V_2O_5, favoring the formation of vanadates.

Besides monovanadate and polyvanadate, alternative species also have been suggested. The existence of an additional three-dimensional polyvanadate overlayer has been proposed by García-Bordejé et al. [15]. Le Bars et al. [21] suggested the formation of dimeric vanadate species on γ-alumina that were reported to be more active in the oxidative dehydrogenation of ethane than the monovanadates formed on silica, due to better reducibility. Recently, Weckhuysen and coworkers [22,23] proposed a completely different umbrella-like vanadate structure with only one bond to the support, consisting of one V=O unit and one peroxide species, as the only existing vanadate species at low and moderate V loadings. In view of a low-temperature adsorption study of oxygen on reduced $V_2O_3(0001)$ surfaces by Abu Haija et al. [24], the existence of peroxide species under catalytically relevant conditions seems doubtful. However, the adsorbed species on the latter surface is quite different from the 'VO_4 upside-down unit' suggested in [22,23].

It should be noted that all of the structural concepts cited above assume V(V) as the only existing oxidation state under oxidizing conditions as they appear during, for example, catalyst calcination in air. However, a number of temperature-programmed reduction (TPR) studies have reported H/V ratios (the ratio of consumed hydrogen atoms per vanadium atom in the measurements) significantly greater than 1 but less than 2. These are the expected values for the reduction of V(V) to V(IV) or V(III) by H_2, respectively. These results were, without experimental evidence, often interpreted as incomplete reduction (e.g. [25–30]). Using X-ray photoelectron spectroscopy (XPS), electron spin resonance spectroscopy (ESR), or UV–vis spectroscopy, considerable fractions of V(IV) were detected in active vanadia catalysts. For instance, Matralis et al. [31] reported V(IV) fractions of 40–80% for vanadate catalysts and of 20–25% for those containing V_2O_5 crystallites on various titania–alumina supports. Pieck et al. [6] measured V(IV) fractions of 20–40% in VO_x/ZrO_2 catalysts and, consistently with [31], an increase of the oxidation state when the monolayer coverage was exceeded. Enache et al. [32] obtained V(IV) fractions of 40–56% on VO_x/TiO_2 and VO_x/ZrO_2 samples. Significant V(IV) amounts, which increased with increasing calcination temperature, were also observed by Reddy et al. [33,34] in VO_x/Al_2O_3, VO_x/Ga_2O_3–TiO_2, and VO_x/La_2O_3–TiO_2 catalysts.

Summarizing these findings, a critical examination of the postulation that V(V) is the only component in active vanadia phases seems mandatory. The present paper aims to do this through a systematic comparison and analysis of TPR and XPS data for γ-alumina-supported vanadium oxide catalysts with varying V contents. Additional analytical techniques, including X-ray diffraction (XRD), diffuse reflectance infrared Fourier transform spectroscopy (DRIFTS), and temperature-programmed desorption (TPD) of pyridine, were also applied, and the performance of the catalysts in the partial oxidation of ethane in a laboratory fixed-bed reactor was tested. The results obtained are discussed in context with the structure of vanadia species on γ-Al_2O_3, and a new proposal regarding this structure is made.

2. Experimental

2.1. Catalyst preparation

The catalysts for this study were prepared by impregnation of γ-alumina (Sasol, purity >97%) with vanadyl acetylacetonate, $VO(acac)_2$ (VWR). The γ-alumina support was selected due to its higher ability to disperse vanadia as compared with SiO_2 [14] and the better thermal stability compared with TiO_2 (at temperatures above 500 °C, vanadia catalyses the conversion of anatase to rutile, yielding a rapid loss of porosity [35,36]). The γ-alumina was grounded in a laboratory mill down to a particle diameter of 20–30 μm before use. The resulting powder had a specific surface area of 200 m^2/g, which decreased to 184 m^2/g after calcination at 700 °C. Its average pore di-

Table 1
The prepared catalyst samples

Catalyst No.	V content (wt%)	C content (wt%)	BET surface area (m^2/g) (fresh/used catalysts)	Theoretical V surface density (atoms/nm^2)[a]
1	1.7	0.07	182/164	1.23
2	2.4	0.25	171/149	1.92
3	4.8	0.16	164/157	3.61
4	6.1	0.21	160/147	4.92
5	9.5	n.d.	12.5/8.8	127
6	11.7	0.01	6.6/9.4	146
7	13.1	0.01	4.3/6.2	250
8	15.7	0.02	19.8/21.0	88.4
V_2O_5	–	–	3.9	597.2[b]

[a] On base of the BET surface area of the tested catalysts.
[b] On base of the BET surface area of the fresh sample.

ameter was measured as 12 nm. Thermal stability of the porous framework is given up to 900 °C, and only after exposure above 1000 °C was a pronounced sintering observed.

For catalyst preparation, γ-alumina and $VO(acac)_2$ were mixed together in acetone, and the resulting suspensions were refluxed under vigorous stirring for 4 h. Then the solvent was evaporated, and the residual solid was dried overnight at 130 °C. Finally, the catalyst precursors were calcined in air at 650 °C for 8 h. Table 1 summarizes the different catalysts prepared for this study. Their V loading was 1.7–15.7 wt%, as measured by AAS. With increasing V doping, the color of the calcined samples varied from light-yellow to grey-green to orange. In some of the catalysts, small amounts of coke were found after calcination (with a maximum at 2–6% V) originating from decomposition of the acetylacetonate ligand. The slightly enhanced surface area of sample 8 compared with samples 5, 6, and 7 is possibly due to its somewhat higher amount of residual carbon, which is supported by the fact that when NH_4VO_3 is used as a vanadia precursor, no increase in surface area was observed for the highest loadings. The reference material V_2O_5 (VWR) was used without further pretreatment.

2.2. TPR and TPO

TPR and TPO (temperature-programmed oxidation) experiments were performed with a BEL-CAT chemisorption apparatus (BEL Japan) that consists of a gas mixing unit allowing both continuous and pulsed reactant dosing (all gases: Westfalen Gas AG), an U-tube quartz microreactor with a thermocouple placed inside the sample, and a thermal conductivity detector (TCD) connected to the inlet and the outlet of the microreactor. The linearity of the TCD response was proven by the injection of gas pulses of various known compositions, and the quantitative hydrogen consumption was calibrated in every measurement by a series of calibration gas pulses.

The sample weight for TPR/TPO was varied between 100 and 400 mg depending on the V loading, to reach similar signal intensities. Details of the pretreatment procedures are given below together with the obtained results. All TPR runs were done with a gas mixture of 10% H_2 in Ar and the TPO runs with 4% O_2 in He, both with a flow rate of 25 ml/min. The heating rate was 3 K/min for all TPR and 5 K/min for all TPO experiments as the best compromise between thermal equilibration of the samples and width of the reduction and oxidation peaks. These heating rates are slower than those usually reported in the literature (typically 6–10 K/min). The absolute error in the average oxidation state of the samples, as determined from the TPR experiments, is estimated to be around 0.1.

2.3. XPS

XPS spectra were recorded using a multipurpose UHV surface analysis apparatus (SPECS, Germany), which provides the possibility of "fast-transfer" XPS measurements within <5 min between the start of the evacuation of the load lock and the first XPS spectrum recorded at a pressure $<5 \times 10^{-9}$ mbar. Thus, short-time UHV-induced changes in the oxidation state of the samples can be monitored, which are not visible for longer transfer procedures requiring usually tens of minutes. A standard high-intensity X-ray source (XR-50, SPECS) has been used in a "stop-and-go" mode to reduce sample irradiation only to the time of data acquisition (MgK_α, excitation energy 1253.64 eV, operation power <200 W). High-resolution spectra (pass energy 10 eV, step size 0.1–0.2 eV) were registered using a hemispherical electrostatic energy analyzer (PHOIBOS-150, SPECS), which provides the possibility of simultaneous photoelectron detection on 9 channels and allows fast data acquisition times (0.5 s per data point). The percentages of V(V), V(IV), and V(III) were determined by deconvolution of the V $2p_{3/2}$ peak using Voigt functions and a Shirley background subtraction (CasaXPS software package [37]). The average error in the oxidation state is estimated to be about ±5% as a result of the precision of the determination of reference binding energies and the deconvolution procedure.

2.4. Additional characterization of the catalysts

Along with TPR/TPO and XPS, the catalysts were characterized by means of atomic absorption spectroscopy (AAS), carbon analysis, nitrogen porosimetry (BET method), XRD, DRIFTS, and TPD of pyridine. AAS analysis of the doping degree was performed using a Varian SpectrAA 250 Plus instrument after microwave extraction of the samples in HNO_3. The carbon content after calcination was determined with a C–H–N analyzer (CHN-1000, Leko). The specific surface area of all catalysts was measured with a Quantachrome Nova 2200e instrument using the multipoint BET analysis method.

XRD patterns of the fresh catalysts and of those reduced by hydrogen in TPR were recorded with a PANalytical X'Pert PRO apparatus using CuK_α radiation. The 2θ range was varied between 10 and 80°, with a step size of 0.016°. Samples were commonly analyzed under air at room temperature. In addition, the supports and selected fresh catalysts were heated in the high-temperature chamber up to 650 °C under air to check for changes in the phase composition at reaction temperatures.

DRIFT spectra were measured for the fresh catalyst powders at room temperature using a Bruker IFS 120 HR spectrometer

and a Collector diffuse reflectance unit with a high-temperature, high-pressure chamber (Thermo Spectra-Tech). Data were collected for 20 min (800 scans) at a resolution of 2 cm^{-1} with a liquid nitrogen-cooled MCT detector and ratioed against a beam with a mirror in place of the sample.

TPD experiments with pyridine were performed in the same BEL-CAT chemisorption apparatus used for the TPR and TPO measurements. The standard procedure consisted of pretreatment, saturation, and desorption steps. Pretreatment was performed in air at 600 °C for 2 h, followed by a 1-h He purge at the same temperature to have the catalysts in a similar hydroxylation state as under operational conditions. After pretreatment, the samples were cooled in He to 130 °C and saturated with 50 pulses of pyridine vapor. After saturation, the samples were flushed at 130 °C for 15 min to remove only physisorbed pyridine. Afterward, desorption analysis was started in a flow of 25 ml/min He at the same heating rate as in the TPR experiments.

2.5. Activity measurements

The performance of the catalysts in the catalytic oxidation of ethane was measured at 450–630 °C (step width of 25–30 °C) at a gas hourly space velocity (GHSV) of 46 000 h^{-1}. For catalytic testing, 0.5 g of each catalyst were inserted into the reactor and fixed with quartz wool. The reactant mixtures were 0.7% ethane and 0.35% O_2 for a lean oxygen-to-hydrocarbon ratio and 0.7% ethane in air for oxygen-excess conditions. The fixed-bed reactor setup with GC-TCD/MSD for product analysis was described previously [38–40]. For an efficient suppression of wall reactions, the reactor walls were passivated with quartz tubes pasted into the steel segments. Gas samples were taken from the inlet and the outlet of the reactor, far enough from the hot reaction zone to avoid reactions within the sampling capillaries. The complete plant was fully automated using the Siemens Simatic Step 7 process control system.

3. Results and discussion

3.1. Catalyst properties

The nature of the active phase in the fresh catalysts was investigated by XRD, DRIFTS, and TPD of pyridine. The XRD patterns, including those of the uncalcined and calcined supports as well as of V_2O_5 for reference, are presented in Fig. 1. The only broad and weak reflections of the original support material indicate the presence of a microcrystalline (crystallite size $\leqslant$5 nm) and of an amorphous fraction. Its diffraction pattern remains unchanged even after thermal treatment at 650 °C, thus excluding temperature-induced changes during calcination.

For the catalysts up to a V loading of 6.1 wt%, corresponding to a V density of 4.9 atoms per nm^2, the obtained diffractograms are identical to that of the support, and no reflections are seen that can be attributed to any other phase. This indicates that in these catalysts, in agreement with published data [15,18,19], vanadia is present primarily as vanadate, which is known to be X-ray amorphous.

For the catalysts with V loadings of 9.5 wt% and above, sharp V_2O_5 reflections appear (library file 00-009-0387 [41]), a hint that the monolayer coverage is significantly exceeded. As indicated by the BET measurements, the presence of V_2O_5 is accompanied by clogging of the pores; the specific surface area of the higher-loaded samples was found to be more than one order of magnitude lower than that of the samples up to 6.1 wt% V loading and that of the original γ-alumina support (compare Table 1). Interestingly, the appearance of the V_2O_5 phase is connected to changes in the crystallinity of the support. The majority of reflections in the XRD patterns of the catalysts with 9.5–15.7 wt% V that are not related to V_2O_5 can be attributed to γ-alumina (library file 00-046-1215 [41]). This indicates that the V_2O_5 not only physically blocks the pores, but also induces crystallization of the amorphous alumina fraction and rapid growth of crystallite size. The formation of $AlVO_4$ (library file

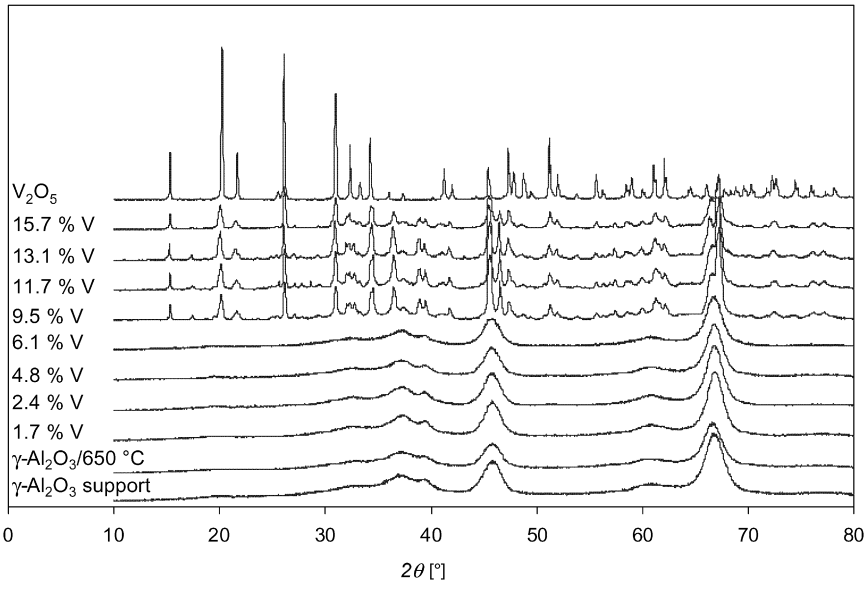

Fig. 1. XRD patterns of γ-alumina-supported catalysts including reference patterns of the bare support with and without thermal treatment at 650 °C, and of V_2O_5.

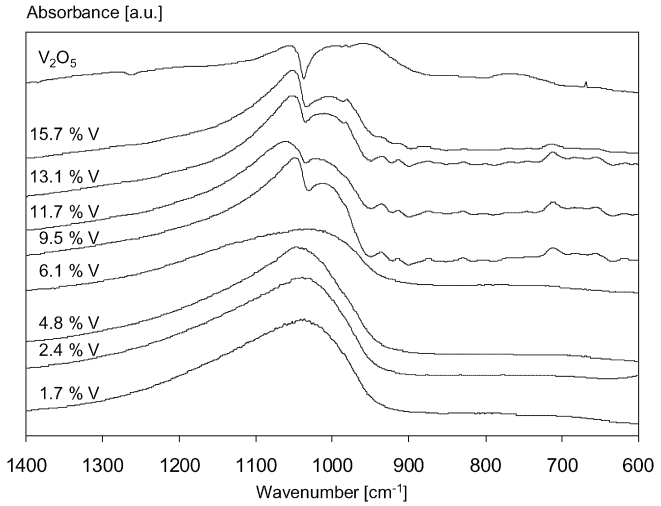

Fig. 2. DRIFT spectra recorded at room temperature for the fresh catalysts and pure V_2O_5.

00-18-0074 [41]) was also observed, because some small reflections due to this compound can be detected. However, it should be noted that the main $AlVO_4$ reflections interfere with those from γ-Al_2O_3 or V_2O_5, making phase identification difficult.

No changes in the XRD patterns were observed after heating to 650 °C compared with those recorded at room temperature. Thus, the crystal structure obtained after calcination appears to be stable on further exposure to reaction temperatures.

Fig. 2 shows DRIFT spectra of the catalysts as well as of pure V_2O_5 at 1400–600 cm^{-1}, where most of the vanadia-related vibrations can be observed. The γ-alumina support has no significant absorption in this wavenumber range. Pure V_2O_5, included as reference, exhibits absorption at around 1052, 1000, 980, 951, and 754 cm^{-1}. According to Magg et al. [42,43], the band at 1052 cm^{-1} to the V=O stretching mode and the vibration at 754 cm^{-1} can be attributed to the V–O–V stretch. The vanadate catalysts with V loadings of 1.7–6.1 wt% V exhibit only one strong absorption, at around 1035–1040 cm^{-1}, which can be attributed to the V=O stretching mode vibration, in good agreement with [42–44]. In contrast, the catalysts with V loadings of 9.5–15.7 wt% V—which, according to the XRD analysis, contain crystalline V_2O_5—show significant absorption at around 1045–1065, 1010, and 980 cm^{-1} (partially only as a shoulder), whereas the weaker V_2O_5 feature around 754 cm^{-1} is not visible. However, weak but reproducible features appear at around 934, 911, 835, 708, and 651 cm^{-1}. Following the foregoing assignment, the band at 1045–1065 cm^{-1} is due to the V=O stretching mode of V_2O_5 crystallites, whereas the band at 708 cm^{-1} indicates the presence of vanadate multilayers. The band at 934 cm^{-1} can be attributed to Al–O–V vibrations, indicating a significant interaction between γ-alumina and vanadia in the high-loaded catalysts as well [42,43,62]. Comparing the catalyst spectra of the high-loaded samples with the V_2O_5 spectrum shows that the absorptions at 1010 and 980 cm^{-1} also can be related to V_2O_5 crystallites. Thus, for these samples, the presence of several vanadia species can be concluded: species bound to γ-alumina, vanadate multilayers, and V_2O_5 crystallites, which are responsible for the V_2O_5 reflections in the XRD patterns.

For the V_2O_5-containing catalysts, additional absorption bands were found at 1965–1970 and 2010–2020 cm^{-1} that can be attributed to overtones of the bands at 980 and 1000–1020 cm^{-1}. Additional strong and very broad absorptions are present at ∼3450 cm^{-1} for both vanadate- and V_2O_5-containing catalysts, which are attributed to surface hydroxyl groups or chemisorbed moisture [29,33,45].

Although the XRD and DRIFTS experiments help to distinguish between vanadate- and V_2O_5-containing samples, they do not allow discrimination between isolated and polymerized vanadate species. Here, besides Raman spectroscopy [46], evaluating the catalyst acidity can be helpful. Le Bars et al. [45] reported that vanadate on alumina catalysts at low loadings has only Lewis and Brønsted acid sites similar to the support, whereas at loadings >1.6 wt% V (1.4 V/nm^2), a significant fraction of weaker Brønsted acid sites appear. Similar observations were made by Blasco et al. [47]; however, here weaker Brønsted acidity was first detected at a loading of 4.3 wt% V (3.7 V/nm^2). It appears that the acidic properties of isolated and polymerized vanadates differ and can be used for phase discrimination.

In the present study, TPD of pyridine was used to characterize the acidity of the samples. It is known that pyridine chemisorbs more strongly at Brønsted acid centers than at Lewis acid centers [48–51]. Using FTIR spectroscopy as well as K blocking of the Brønsted acid sites, these studies found that pyridine chemisorbed at Lewis acid sites desorbs at temperatures already below 300–400 °C without any reduction of the catalyst. In contrast, pyridine bound to Brønsted acid sites is removed only at higher temperatures under decomposition, accompanied by vanadia reduction. This finding is supported by experiments with bare support materials. In contrast to Al_2O_3 and TiO_2, silica is known to exhibit no significant Lewis acidity [52]. Whereas Al_2O_3 and TiO_2 are characterized by pyridine TPD patterns already well below 500 °C, no pyridine-related signals appear in this temperature range for silica. Here only one desorption peak is observed, with a maximum at 730 °C, indicating the presence of strong Brønsted acid sites.

The bare γ-Al_2O_3 support exhibits three pyridine desorption peaks at 185, 350, and 730 °C. The first two signals thus can be attributed to medium and strong interaction with Lewis acid sites, whereas the latter can be related to strong Brønsted acidity. He-TPD without pyridine chemisorption verified that the signals are truly caused by pyridine exposure, not by any other effects.

Fig. 3 shows the TPD patterns for the catalysts and for the V_2O_5 reference. Two peaks at 180–190 and 350–410 °C related to Lewis acidity are present in all patterns, including that of V_2O_5. Thus, the strength of Lewis acidity is rather independent of the nature of the vanadia species, and only the density of Lewis acid sites increases by a factor of 2–3 due to the appearance of V_2O_5 crystallites. More interesting changes can be observed in the region above 400 °C, attributed to desorption of pyridine from Brønstedt acid sites. For the catalyst with 1.7 wt% V, only an increase in pyridine desorption beginning at

>600 °C is observed. This signal is more pronounced than for the support, suggesting a rather strong acidity of the V species for this low-loaded catalyst, contrary to the results reported in [45,47]. The desorption peak at >600 °C is also found for the 2.4% wt% V sample, but decreases significantly at a loading of 4.8 wt% V and finally disappears for the 6.1 wt% V sample, the vanadate catalyst with highest loading. However, starting at 2.4 wt% V, a new desorption peak at around ∼500 °C that increases continuously with V loading can be detected. Thus, for the vanadate catalysts with increasing V loading, the strong Brønstedt acid sites are gradually replaced by sites of less strong character, indicating the existence of two different vanadate species.

For the samples containing V_2O_5 crystallites (9.5–15.7 wt% V) and for pure V_2O_5 itself, the strength of Brønstedt acidity is similar to that of the 1.7 wt% V sample. Thus, the pyridine desorption peak at 500 °C disappears, and that at above 600 °C returns. Moreover, the density of Brønsted acid sites seems to be similar. After the pyridine TPD experiments, all catalyst samples changed to a blue-green color, corresponding to a significant reduction of V(V) to V(IV) by pyridine due to decomposition of the latter.

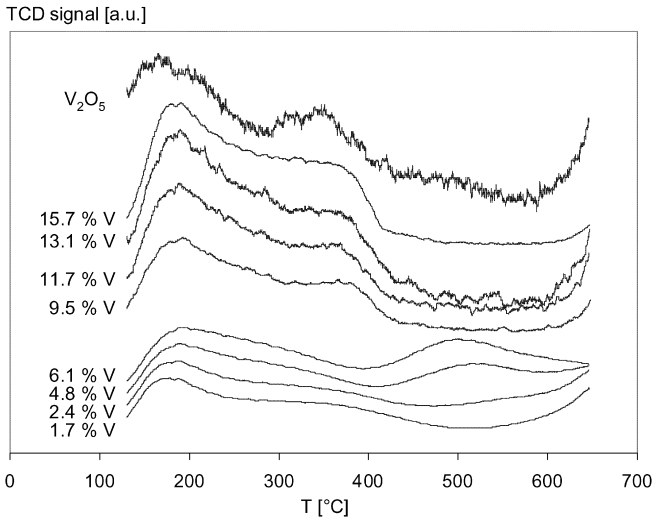

Fig. 3. Pyridine TPD patterns of the fresh catalysts. Experimental conditions: pretreatment in air at 600 °C/2 h, 50 pulses of pyridine at 130 °C, TPD with 25 ml/min He, 3 K/min up to 650 °C. All curves are normalized with respect to sample weight and surface area.

The foregoing observations on the existence of two different vanadate phases are also supported by transmission electron microscopy (TEM) images of two VO_x/γ-Al_2O_3 reference samples prepared as described earlier (see Fig. 4 [53]). The sample with 1.4 wt% V shows only amorphous structures related to vanadia. In contrast, the sample with 5.0 wt% V, which is still free of V_2O_5 crystallites, exhibits well-ordered regions in the range of tens of nm.

Summarizing our findings, it seems that the 1.7 and 2.4 wt% V samples (<2 V/nm^2) are characterized primarily by isolated amorphous vanadate species, while in the 4.8 and 6.1 wt% V (3.6–4.9 V/nm^2) catalysts, well-ordered polymerized vanadate is dominating. Crystalline V_2O_5 is present at V loadings of 9.5–15.7 wt% V; this is in accordance with [14,16–19]. The following sections report investigations of reducibility, oxidation states, and redox cycles of these different phases by TPR and XPS.

3.2. TPR and TPO studies

3.2.1. Initial reducibility

The reducibility of catalysts can be evaluated by TPR using hydrogen diluted in argon as a reactant. It is widely accepted that low reduction temperatures correspond to a high degree of V dispersion [54–56], and thus that the different vanadia phases can be well distinguished within a TPR pattern. Only for very low V loadings or weak vanadia–support interaction (as for silica) is the reduction temperature reported to increase again, which is attributed in [46,57,58] to the presence of an ultra-dispersed V species. In addition, by quantifying hydrogen consumption and its correlation to the degree of metal doping, it is possible to calculate the original or final average oxidation state of the sample if the corresponding reference state is known. This is explored in Section 3.4.

Two series of initial TPR experiments were performed with the fresh catalysts using different pretreatments. In the first se-

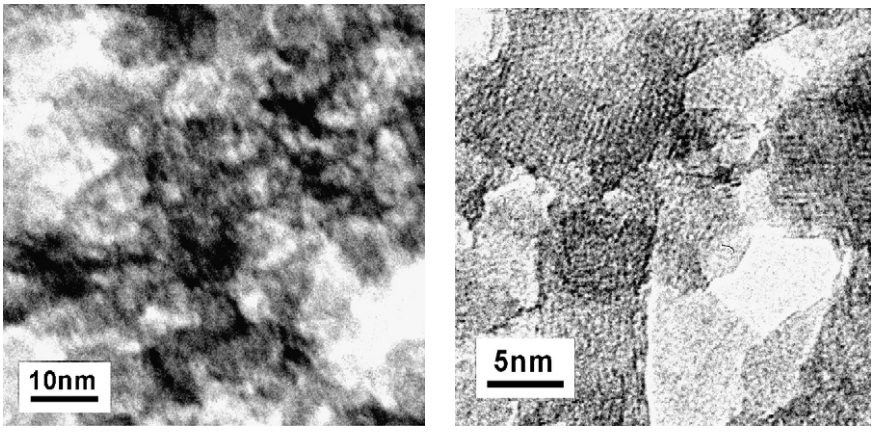

(a) (b)

Fig. 4. TEM images of 1.4 (a) and 5.0 wt% V (b) on γ-alumina support. Microscope: Philips CM 200 LaB_6 (by courtesy of [53]).

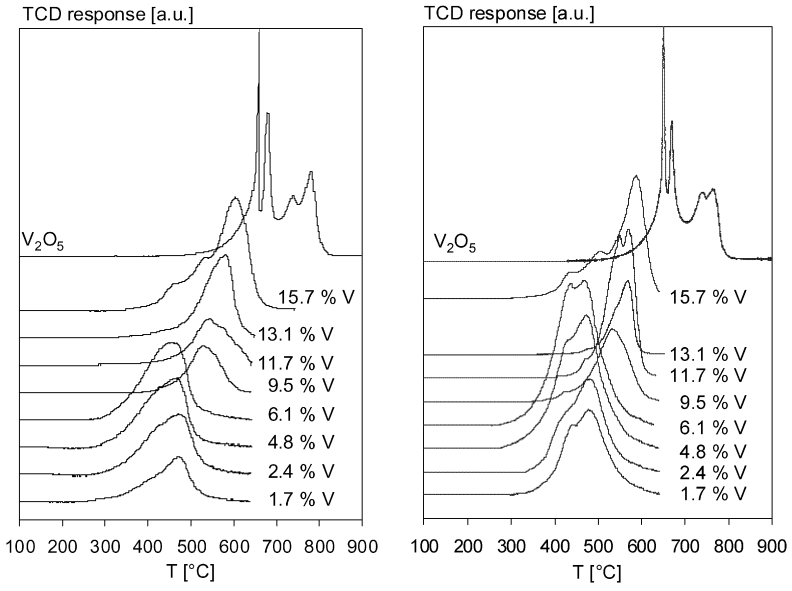

Fig. 5. TPR patterns of the fresh catalysts. Pretreatment: (a) 3 h in He at 250 °C, (b) 2 h in air at 600 °C for 2 h both followed by 1 h in He at the same temperature. TPR measurement: 25 ml/min 10% H_2 in Ar, heating rate 3 K/min.

ries, samples were pretreated in 50 ml/min He at 250 °C for 3 h to remove the absorbed moisture; in the second series, samples were pretreated in 50 ml/min air at 600 °C for 2 h, followed by a 1-h He purge at the same temperature to destroy any remaining organic impurities. The corresponding TPR patterns are shown in Fig. 5. Their quantitative analysis is discussed in Section 3.4.

For V_2O_5, in both series of experiments, reduction peaks appear at ∼660, ∼681, ∼741, and ∼783 °C. This is in a range comparable to the data reported in [29,30]. However, due to the fact that the patterns obtained in TPR are rather sensitive to the experimental conditions (apparatus, heating rate, and sample weight), the number of peaks differs in the publications.

For the vanadate catalysts with V loadings up to 6.1% V, two reduction peaks can be observed with maxima at 430–440 and 470–480 °C. In the case of He pretreatment, the first reduction peak appears only as a shoulder of the latter, in contrast to air pretreatment, where this peak is significantly more pronounced. This indicates that these most-reducible V species are formed only after the organic ligands are removed. Note that the peak at 430–440 °C increases with increasing V loading. In the literature, often only the high-temperature reduction peak, commonly found at 460–520 °C, is reported [26,28,54,59].

For the higher-loaded V_2O_5-containing samples, the two vanadate reduction peaks are only barely visible. Here the main reduction peaks can be found at 530–550 and 580–610 °C, with the latter peak increasing with increasing V loading. No significant differences are found for He and air pretreatment.

In agreement with the literature (see e.g. [27,30]), it is evident that the V_2O_5-containing catalysts are more difficult to reduce than the vanadate-containing samples, parallel to the decreased degree of V dispersion. Apparently, the presence of peaks at temperatures above 500 °C can be used as an indicator for the presence of agglomerated (bulk-like) V_2O_5 phases. However, the reduction temperature of the V_2O_5-containing catalysts is still lower than that of pure V_2O_5, indicating a significant interaction of the crystalline V_2O_5 phase with the support as well, consistent with the DRIFTS experiments.

From Arrhenius plots calculated from the TPR patterns, activation energies of 80–100 kJ/mol for vanadate reduction and 140–180 kJ/mol for the V_2O_5 phases can be estimated. A similar value for vanadate reduction was recently published by Kanervo et al. [60]; for V_2O_5 phase reduction, these authors reported an activation energy of 119 kJ/mol, somewhat lower than in our experiments but still larger than for vanadate.

In recent theoretical studies, Todorova et al. [61] and Brázdová et al. [62] investigated the reducibility and other properties of vanadia films and of V_2O_5 clusters on α-Al_2O_3(0001) surfaces. In these papers, reducibility was defined as the energy of oxygen defect formation at the catalyst surface and correlated to the catalytic activity, assuming that the latter depends on the catalyst's ability to release lattice oxygen following the Mars–van Krevelen mechanism [67]. These authors found that reduction of small V_2O_5 vanadia clusters on α-Al_2O_3(0001) should be more difficult than reduction of the (001) V_2O_5 single-crystal surface but significantly easier than reduction of thin vanadia films on this support [62]. This is in an apparent contradiction to the findings of the present study, where TPR experiments showed that ultra-thin vanadia films on amorphous γ-alumina supports are reduced more easily by hydrogen than V_2O_5-containing phases, and that bulk V_2O_5 is the most difficult to reduce under these conditions. However, although the discrepancy between the studies may be due to the different support materials, it seems more likely that it stems from the other authors' definition of "reducibility" as being related to the energy of defect formation, whereas in the intuitive, qualitative "chemists' interpretation" reducibility includes both kinetic and thermodynamic contributions (i.e., activation energies as well

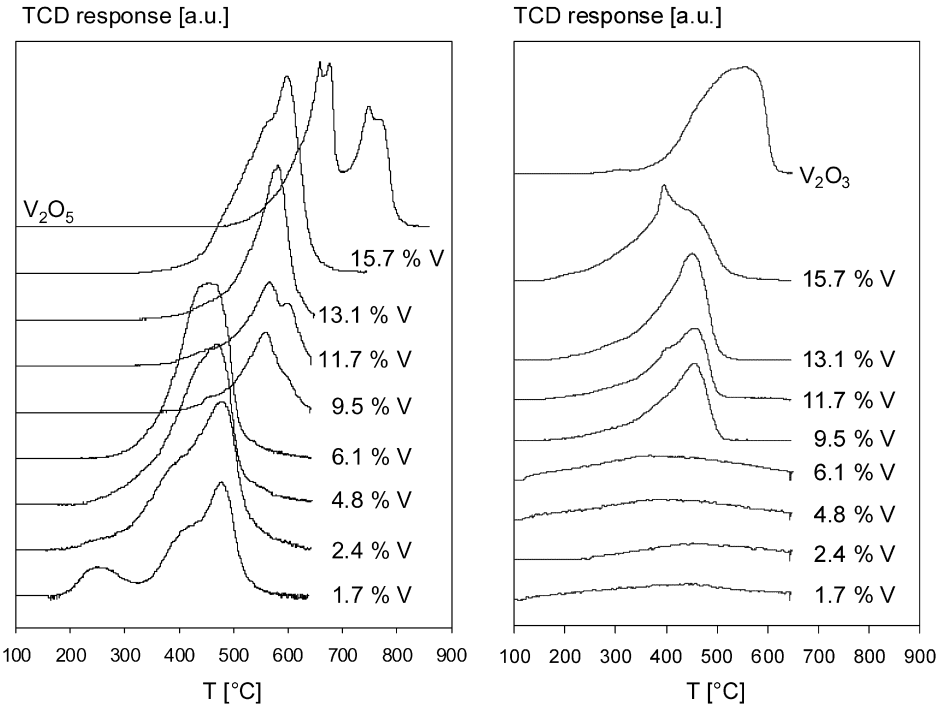

Fig. 6. TPR–TPO redox cycles: (a) TPR patterns from the third run; (b) TPO patterns from the second run. Pretreatment in all TPR and TPO runs: 3 h in He at 250 °C. TPR measurement: 25 ml/min 10% H_2 in Ar, heating rate 3 K/min. TPO measurement: 25 ml/min 4% O_2 in He, heating rate 5 K/min.

as enthalpies). We have shown above that the activation energy for vanadate reduction by hydrogen is significantly lower than that for the V_2O_5 phases.

It also should be noted that the catalytic activity found in our investigation is higher for ultra-thin vanadia layers than for V_2O_5 crystallites, and can be correlated to the degree of directly accessible V(V) sites (see Section 3.5).

3.2.2. *Catalyst changes in H_2-reduction/O_2-reoxidation sequences*

It is known that the V dispersion and the fractions of the different vanadia phases can change due to prolonged thermal treatment, after passing through several redox cycles [54], or under working conditions. Under reaction conditions, the Tammann temperature is exceeded significantly, so that significant surface mobility of vanadia becomes likely [63]. This can even cause changes in the nature of the surface species, as reported by Ballarini et al. [64]. To investigate such changes, we exposed the catalysts to different reducing and oxidizing environments at elevated temperatures. Two types of experiments were carried out: (I) H_2-TPR–O_2-TPO redox sequences, introduced in this section, and (II) pretreatment with different diluted ethane–oxygen mixtures to simulate catalyst operation in the catalytic oxidation of hydrocarbons, discussed in the next section.

During the TPR–TPO redox cycles, the He pretreatment procedure (3 h in He at 250 °C) was applied for both TPR and TPO as described in the previous chapter, to avoid thermally induced structural changes during the pretreatment step. For each catalyst, the sequence TPR–TPO–TPR–TPO–TPR was studied. Fig. 6 shows the patterns from (a) the third (i.e., last) TPR run and (b) the second TPO run.

Comparing the third and first TPR run (Fig. 6a vs. Fig. 5a) reveals several changes that depend on the V loading. For the catalysts with isolated V species (1.7 and 2.4% wt% V), the area of the reduction peaks at 430–440 and 470–480 °C decreases, and a new low-temperature peak appears already at around 250 °C. The latter increased with increasing number of reduction–reoxidation cycles. In contrast, the polyvanadate catalysts with V loadings of 4.8 and 6.1 wt% V show no significant changes in the corresponding TPR patterns. For the catalysts with V loadings of 9.5–13.1 wt%, the vanadate shoulder becomes slightly more visible. The area of the other peaks remains nearly constant; however, the position of the peak originally located at 530–550 °C shifts by about 30 K toward higher temperatures, whereas in contrast, the second V_2O_5 reduction peak remains at nearly the same position (600–610 °C). For the catalyst with 15.7% V the peak at 460 °C disappears, while the one at 535 °C shifts to 575 °C and increases in intensity, indicating growth of the V_2O_5 crystallites on this catalyst. The area of the third reduction peak at 605 °C remains nearly constant.

The TPO patterns from the reoxidation, reported in Fig. 6b, are rather flat, especially for the reduced vanadate catalysts, where only a weak maximum close to 400 °C is observed. The higher-loaded catalysts show two more pronounced oxidation peaks with maxima at ∼400 and 430–450 °C, respectively. Apparently, reoxidation occurs at lower temperatures than reduction, as was also e.g. found by Le Bars et al. [65]. Consequently, its activation energies are significantly lower than those of re-

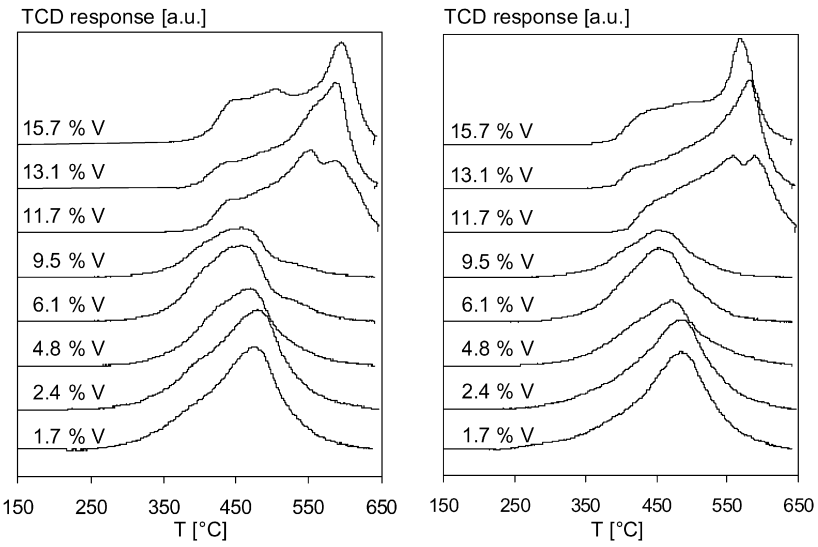

Fig. 7. TPR experiments with 'time on stream' pretreatment at 600 °C. Pretreatment gases: (a) 0.7% ethane in air, (b) 7% ethane and 3.5% oxygen in He. TPR measurement: 25 ml/min 10% H_2 in Ar, heating rate 3 K/min.

duction: 20 kJ/mol for the dispersed and 40 kJ/mol for the bulk-like vanadia phases, respectively.

Note that the appearance of a more reducible phase due to H_2-reduction–O_2-reoxidation sequences is not limited to low-loaded VO_x/γ-Al_2O_3 catalysts. Similar changes were also found for silica- and titania-supported samples; it seems that H_2/O_2 redox cycles strengthen the interaction between V and the support. Partially contradictory studies can be found in the literature. Gervasini et al. [54] reported no structural changes for their γ-alumina- and silica-supported vanadia catalysts but significant alterations for their catalysts on titania support, accompanied by a loss of reducible species (TPR and TPO up to 527 °C). In contrast, Besselmann et al. [56] performed redox cycle experiments with various VO_x/TiO_2 Eurocat samples and observed no structural changes (TPR up to 600 °C, TPO up to 450 °C). Similar results were reported by Arena et al. [66], who investigated the reducibility of vanadia catalysts on a wide variety of supports in all steps of a H_2/O_2 redox cycle at 367 °C. It seems possible that the structural changes in the present study are due to the higher final temperature (650 °C) in the TPR and TPO runs used herein.

3.2.3. Structural changes of the catalysts after testing in ethane oxidation

The catalytic oxidation of hydrocarbons is assumed to be based on reduction–reoxidation cycles, following the well-accepted Mars–van Krevelen mechanism [67]. Therefore, structural changes of the catalysts can be expected, which also can affect catalyst performance. For this reason, the catalysts under working conditions in the partial oxidation of ethane were also investigated. Note that for this reaction, supported vanadia catalysts are not the most efficient ones and are significantly outperformed by the new class of Mo–V–Nb–Se/Te–O_x catalysts, which can selectively activate sp^3-hybridized but not sp^2-hybridized C–H bonds, leading to efficient suppression of the nondesired consecutive oxidation of ethylene. These Mo–V–Nb–Se/Te–O_x catalysts can be used profitably in the oxidation of ethane to ethylene [68–71] and of propane to acrolein [72–78] as well as acrylonitrile [77,79,80], but not for the oxidative dehydrogenation of hydrocarbons with more than two carbon atoms [81]. For the latter, vanadia catalysts remain the preferred material. However, because the focus of this study is on gaining more insight into vanadia-based catalysts in general, we choose the partial oxidation of ethane, which can be easily monitored by GC analysis, as the test reaction.

To evaluate structural changes of the catalysts in ethane oxidation, before H_2-TPR, the catalysts were pretreated at 600 °C with mixtures of ethane and oxygen at oxygen-to-ethane ratios of 0.5 or 30 (i.e., conditions similar to those in the activity tests). At this temperature, all catalysts have sufficient activity. The pretreatment for the first TPR run was performed with 35 ml/min of 0.7% ethane in air for 2 h to simulate catalyst operation under oxygen-excess conditions. Afterward, the samples were purged for 1 h in 50 ml/min He at 600 °C to remove adsorbed gases, then cooled in He. After the corresponding TPR run, the catalyst samples were reoxidized with 35 ml/min of the same ethane–air mixture for 0.5 h at 600 °C. Next, they were pretreated with 35 ml/min of a mixture of 7% ethane and 3.5% oxygen in He for 2 h at the same temperature, that is, under oxygen-lean conditions, as commonly applied in catalytic tests in the literature. Subsequently, the samples were again purged with 50 ml/min He at 600 °C for 1 h and cooled in He, before the second TPR was started. The patterns obtained from these TPR runs are shown in Fig. 7.

First, note that the TPR patterns obtained after these pretreatments show distinct similarities, suggesting that even under oxygen-lean conditions, no significant reduction occurs and the same vanadia phases are present. This is in agreement with the study of Gao et al. [8] on ethane and butane oxidation, which found that the working catalyst is in the oxidized state

Table 2
Oxidation states evaluated by XPS, and H/V ratios from TPR

	Catalyst No.							
	1	2	3	4	5	6	7	8
V content (wt%)	1.7	2.4	4.8	6.1	9.5	11.7	13.1	15.7
Oxidation state evaluated by XPS	n.d.	4.3	4.3	4.3	4.8	4.8	4.7	4.8
Hydrogen consumption (H/V atomic ratio) in TPR								
Initial TPR pretreatment in He/250 °C	1.2	0.9	0.9	1.3	1.9	1.8	1.7	1.7
Pretreatment in air at 600 °C	0.7	1.1	1.4	1.2	1.7	1.5	1.5	1.7
3rd TPR in TPR–TPO redox sequences	1.3	1.4	1.3	1.4	1.8	1.9	1.7	1.9
Pretreatment 0.7% C_2H_6 in air at 600 °C	1.5	1.4	1.4	1.4	1.8	1.8	1.8	1.8
Pretreatment 7% C_2H_6 and 3.5% O_2 in He at 600 °C	1.4	1.4	1.2	1.2	1.8	1.6	1.6	1.5

in both reactions. However, larger differences can be observed compared with air pretreatment (Fig. 5b) and TPR–TPO sequences (Fig. 6). For all vanadate catalysts, the first reduction peak located at 430–440 °C is moderately decreased relative to the reference TPR with air pretreatment (slightly stronger for lean than for oxygen-excess conditions) and appears only as a shoulder of the second reduction peak at 470–480 °C, which remains nearly unchanged with respect to position and area. This suggests that the peak at 430–440 °C corresponds to the species involved in ethane activation. No difference between isolated and polymerized vanadate species is seen; the reducibility of these two vanadate species also remains comparable after time on stream in the ethane oxidation. In contrast to the H_2-TPR–O_2-TPO redox sequence experiments, the low-temperature peak at 250 °C does not appear. This indicates a full reversibility of the processes described in the previous section, if the catalyst is exposed to a different reaction environment.

In contrast to the vanadate-containing samples, changes in the V_2O_5-containing catalysts after exposure to ethane–oxygen mixtures are much more significant. In particular, the TPR pattern of the 9.5 wt% V catalyst changes almost completely and appears similar to that of the vanadate catalysts, with the main reduction peak at 470–480 °C and a significant shoulder at 430–440 °C. From the original reduction peak at 530–550 °C, only a weak residual signal remains. A new peak at 430–440 °C, along with a shoulder close to 480 °C, also can be identified in the patterns of the catalysts with 11.7–15.7 wt% V. These low-temperature peaks indicate an at least partial transformation of the V_2O_5 phases during time on stream in hydrocarbon oxidation, accompanied by the formation of more reducible and more dispersed species (possibly amorphous vanadia overlayers). The V_2O_5 reduction peaks at 530–550 °C and 580–610 °C are still present for the latter catalysts. The results from the second TPR run can be reproduced when performing the measurements with fresh catalyst material. Two conclusions can be drawn: (I) The phase composition of fresh and working catalysts may differ significantly, and (II) the changes in the catalysts are specific to the reducing agent (hydrogen or hydrocarbon) and are at least partially reversible.

The almost identical amounts of hydrogen consumed in the TPR experiments with the two ethane–oxygen mixtures and in the third TPR within the TPR–TPO sequences (Table 2) indicate that in ethane oxidation under steady-state conditions, the catalysts are in the oxidized state, independent of the nature of the active vanadia phase. This is consistent with the TPO measurements, where the reoxidation started already at 300 °C and was completed at 500 °C (Fig. 6b). Similar observations have been reported by Gao et al. [8] and Le Bars et al. [65]. Quantification of the TPR results is discussed in more detail in Section 3.4.

3.3. XPS results

The XPS investigations in this study were focused on determining the initial vanadium oxidation state for the different catalysts as a reference for interpretating the TPR results. The V(V) and V(IV) contributions were determined from the V $2p_{3/2}$ peak deconvolution, whereas the position of the V(V) peak was calibrated using the photoelectron spectra obtained from a reference sample ($VOPO_4$) with phase structure confirmed by XRD [82]. The measured reference value of 518 eV is in a good agreement with the literature values [83–85] and with our latest measurements performed using a monochromatic X-ray source (FOCUS-500, SPECS) for the same sample embedded in indium foil to minimize charging effects [86]. The foregoing value for V(V) and the value of 516.9 eV for the V(IV) contribution [87] were used for the V $2p_{3/2}$ peak deconvolution for all samples studied herein. The results obtained from the deconvolution procedure were also compared with the average oxidation state calculated from analysis of the splitting between the O 1s and V $2p_{3/2}$ peaks as an independent criterion [88]. Good agreement between these two methods was observed for all samples.

The results from the "fast transfer" XPS measurements, performed under minimized exposure of the samples to UHV conditions and X-rays, are reported in Table 2. The vanadate catalysts (2.4–6.1 wt% V) show initial oxidation states of ∼4.3; those containing V_2O_5 phases (9.5–15.7 wt% V), an initial oxidation state of ∼4.8. All fresh catalysts contain only V(V) and V(IV) species, and no contributions from V(III) can be detected in the XPS spectra.

To evaluate the stability of the different VO_x phases under UHV conditions, selected samples were exposed continuously to UHV for hundreds of hours. The main result of our first investigation [87] was confirmed, that is, a vacuum-induced reduction of the vanadium oxide catalysts could be observed. The oxidation state drops from 4.7–4.8 by ∼0.3 for the high-loaded

V_2O_5 containing samples, but by only 0.15–0.2 (from 4.3–4.35) for the vanadate catalysts, respectively. However, the time scale for this decay is on the order of 100–150 h, and only a negligible decrease is observed within the first 30 min, during which the reference oxidation states for the interpretation of the TPR experiments are determined. Thus, it can be concluded that also previous XPS studies by other authors on γ-alumina-supported vanadium oxide catalysts probably reflect the original oxidation state of the sample and are not significantly influenced by exposure to the reducing vacuum conditions.

When comparing XPS and TPR data, it must be kept in mind that in contrast to TPR, which measures the complete amount of accessible reducible species including deeper layers and is kinetically controlled by hydrogen activation, XPS is sensitive only to a few upper layers of the catalyst surface, and that a reduction under UHV conditions is accompanied by a release of the outermost lattice oxygen species. However, regarding the initial oxidation states, TPR and XPS can be expected to provide consistent results, especially for monolayer catalysts with their thin vanadate layers.

3.4. Initial and final oxidation states in TPR–TPO redox cycles of vanadia catalysts

Besides providing information on the reducibility of the different vanadia phases, TPR allows correlation of H_2 consumption and catalyst oxidation states. Based on stoichiometry, H/V ratios of either 1 or 2 may be expected, corresponding to reduction of V(V) to V(IV) or V(III), respectively. A reduction to lower oxidation states is unlikely due to the high stability of V_2O_3 even at elevated temperatures (see, e.g. [89]). However, as mentioned in the Introduction, often in practice (as in the present study), fractional H/V ratios of 1–2 are measured that cannot be attributed unequivocally to an original or final oxidation state based on the TPR experiment alone. Here, for, example, reference XPS data are needed.

Table 2 summarizes the different H/V ratios for the experiments reported in Sections 3.2.1–3.2.3, together with the XPS data from Section 3.3. Because the comparison of TPR and TPO indicates that vanadia reoxidation occurs faster and at lower temperatures than reduction, it can be expected that the XPS measurements reflect the catalysts in their fully oxidized state after cooling in air. The slightly lower H/V ratios for the fresh catalysts ("initial TPR") in comparison to the "used" ones (pretreatment with oxygen–ethane mixtures and the third TPR in the TPR–TPO sequence) are due to the initial existence of organic residuals from catalyst preparation, evidenced by the significant carbon content in the fresh catalysts (Table 1) and by the CO_2 release observed in the initial period of the catalytic tests. The lower H/V ratios after oxidizing air pretreatment indicate that complete precursor oxidation seems to require intermediate vanadia reduction, and that only after passing through several redox cycles is the "real catalyst" obtained.

Taking the measured XPS data as the initial oxidation state for the TPR experiments, it is evident that hydrogen completely reduces all vanadia phases to the oxidation state +3. The observed H/V ratios of <2—particularly for vanadium loadings of ⩽6.1 wt%—are consistent with the presence of V(IV) in the XPS spectra and unambiguously not due to incomplete reduction of a pure V(V) species. For the higher-loaded samples, this conclusion was also confirmed by XRD measurements of the reduced samples directly after TPR, where V_2O_3 was identified as the only V-containing phase (library file 01-071-0343 [41]).

From these data, it can be concluded that in the dispersed vanadate catalysts, only approximately 1/3 of vanadium is in the oxidation state +5, in contrast to nearly 80% in the catalysts with a V_2O_5 phase. These percentages cannot be enhanced by moderately oxidizing atmospheres (TPO or air pretreatment at 600 °C), which means that the V(IV) fractions are rather stable even under oxidizing conditions. Thus, it can be concluded that in all γ-alumina-supported vanadia catalysts studied herein, two different species of V atoms with different redox behaviors exist: one species that can show the full redox cycle between V(V) and V(III) and another species that undergoes a redox cycle only between V(IV) and V(III). The V(IV)/V(V) ratio in the oxidized state depends on the nature of the vanadia phase present in the catalysts; a V(IV) excess corresponds to highly dispersed vanadates, whereas a V(V) excess corresponds to agglomerated V_2O_5 phases.

Note that the structural changes observed during the H_2-TPR–O_2-TPO redox sequences and for the catalysts "at work" in the ethane oxidation are characterized by changes in the positions of the reduction peaks but not in the measured hydrogen consumption. Consequently, the more reducible phase formed during the interaction of the V_2O_5-containing catalysts with the ethane–oxygen mixtures must be a V(V) phase. This means its chemical nature differs from the mainly V(IV)-containing vanadate phase in the low-loaded catalysts. These conclusions are supported by the catalytic tests on ethane oxidation presented in the next section.

The results given herein are in good agreement with data from Casaletto et al. [90], who compared TPR and XPS results from a series of alumina-supported vanadyl and iron vanadyl phosphate catalysts. From XPS, they found the presence of mainly V(IV) and V(V) and an only minor fraction of V(III) in the fresh catalysts (after 3 h of calcination at 550 or 650 °C in air) and a final oxidation state of +3 after TPR.

3.5. Structure–activity relationships in ethane oxidation

The activity of the catalysts in ethane oxidation was measured at oxygen-to-ethane ratios of 0.5 and 30 (similar to the TPR experiments reported in Section 3.2.3) at 430–630 °C, for a GHSV of 46 000 h^{-1}. The catalytic performance is reported in Fig. 8 for oxygen-lean conditions and in Fig. 9 for oxygen-excess conditions. Ethane conversion, $X_{C_2H_6}$, exhibits the expected correlation to temperature, oxygen supply, V loading, and available surface area. Under lean conditions, oxygen becomes limiting at ethane conversions >30%. The selectivity to ethylene, the main product, decreases with increasing ethane conversion, accompanied by increased selectivity toward CO. The consecutive oxidation of ethylene to CO becomes stronger with increased V loading, particularly for the V_2O_5-containing samples. However, significant direct CO formation from ethane

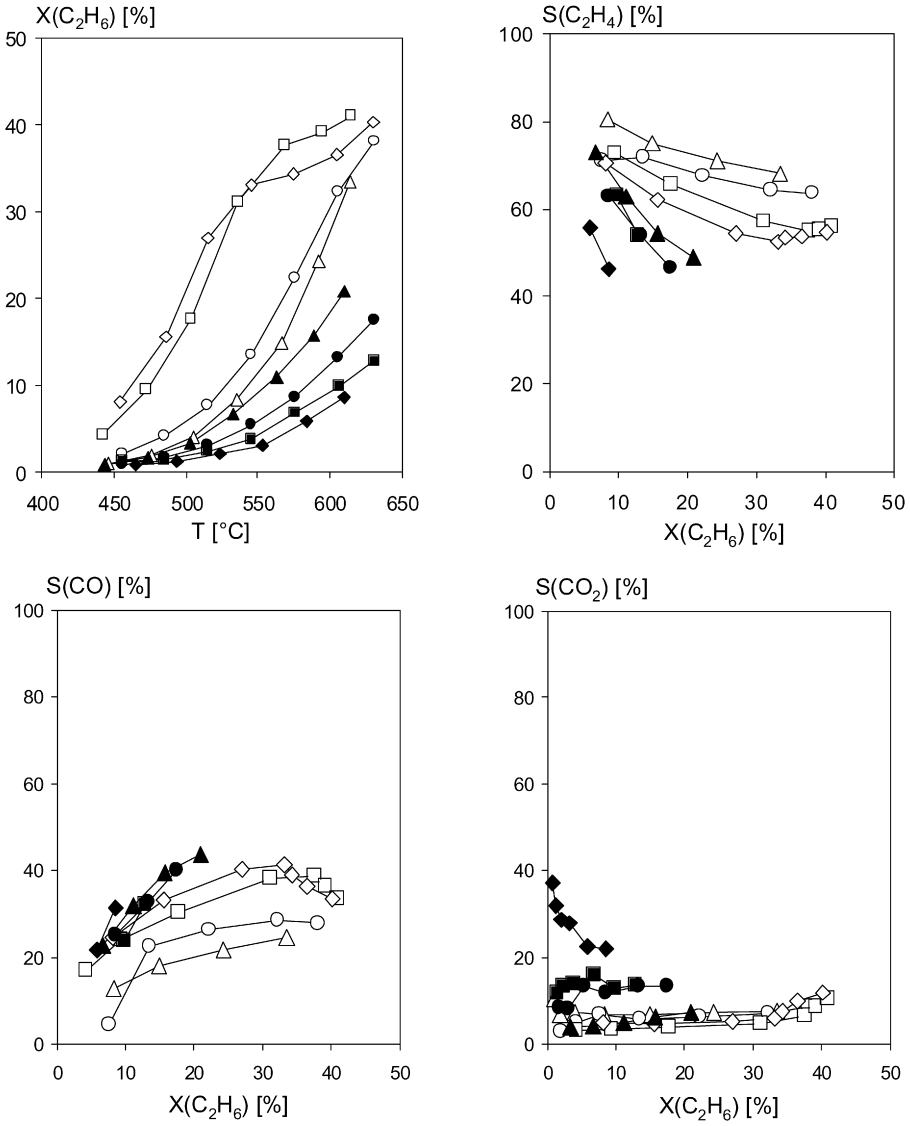

Fig. 8. Catalytic activity of the different catalysts in the oxidation of ethane under oxygen-lean conditions: (△) 1.7, (○) 2.4, (□) 4.8, (◇) 6.1, (▲) 9.5, (●) 11.7, (■) 13.1, and (◆) 15.7% V. Feed composition: 0.7% C_2H_6, 0.35% O_2, balance N_2, GHSV 46 000 h^{-1}.

also occurs. The selectivity toward CO_2 remains rather constant over a wide range of ethane conversion except at the highest V loading of 15.7%, where it rapidly decreases. Thus, up to 30% ethane conversion, CO_2 is primarily formed directly from ethane. The initial product distribution and activation energies for all catalysts are given in Table 3; these activation energies are in good agreement with published data [19].

The highest ethylene yields of 22–24% were obtained for the vanadate catalysts at 630 °C under oxygen-lean conditions. This yield is at the upper end of performance data reported for supported vanadia catalysts (e.g. [19,65,91–94]), whereas the activation energies and the initial product distribution summarized in Table 3 are in the range reported in the literature. Interestingly, the polyvanadate catalysts are less selective for ethylene and more strongly oxidizing toward CO than the catalysts with isolated vanadate species or V_2O_5 crystallites. No coke formation was observed during the ethane oxidation experiments.

Experiments on ethylene oxidation, using a similar set of experimental conditions (0.7% C_2H_4; 1 and 21% O_2; temperature range 430–630 °C; contact time, $W/F = 75$ g s/l), also led to acetaldehyde with catalysts containing V_2O_5, which was not observed in the oxidation of ethane. The acetaldehyde selectivity behaves opposite to that of CO.

It should be mentioned that, as already reported by Heracleous and Lemonidou [95], the bare alumina support has a considerable activity in both ethane and ethylene oxidation, but ethylene formation from ethane is rather poor ($S = 10$–20%, $Y_{max} < 3.5\%$).

CO oxidation to CO_2 was also studied separately, and activation energies of 83 kJ/mol for the vanadate catalysts and 72 kJ/mol for those containing V_2O_5 crystallites were found, in reasonable agreement with earlier reports [96,97]. It should be mentioned that this reaction appears to be strongly inhibited by ethylene, which may be the reason for the low CO_2 selectivity in ethane oxidation.

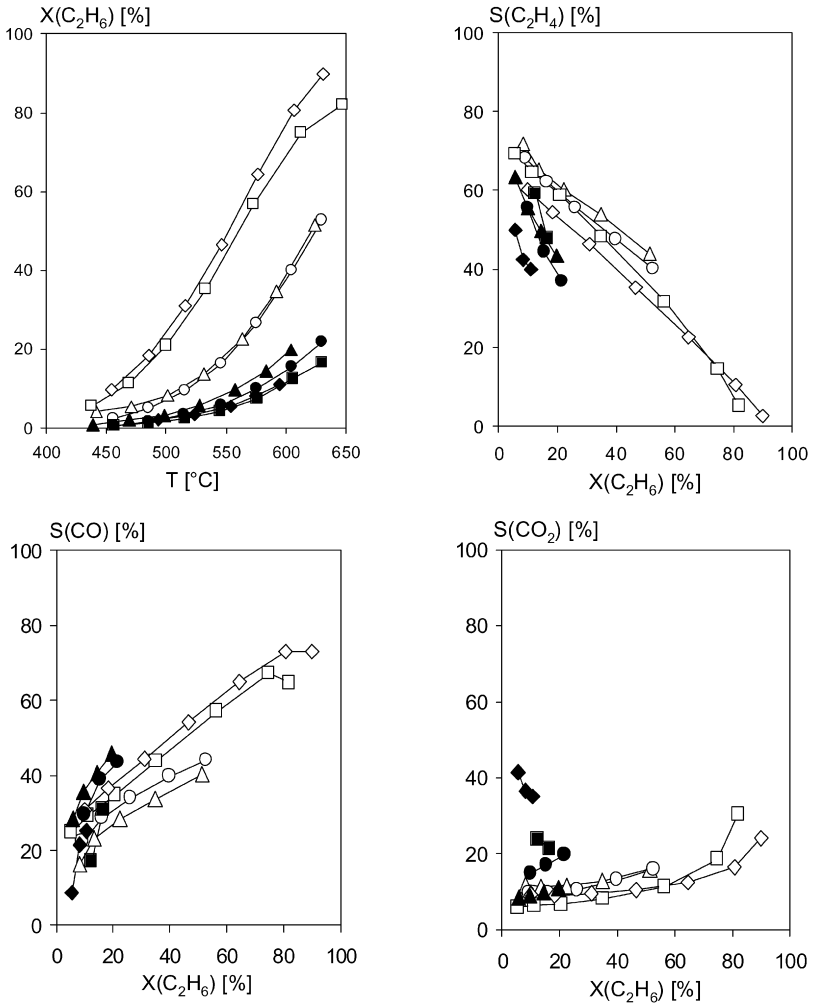

Fig. 9. Catalytic activity of the different catalysts in the oxidation of ethane under oxygen-excess conditions: (△) 1.7, (○) 2.4, (□) 4.8, (◇) 6.1, (▲) 9.5, (●) 11.7, (■) 13.1, and (◆) 15.7% V. Feed composition: 0.7% C_2H_6, 21% O_2, balance N_2, GHSV 46 000 h^{-1}.

Table 3
Activation energies and initial product distribution in the oxidation of ethane and ethylene

V loading (wt%)	Activation energy (kJ/mol)[a]	Initial selectivity at oxygen-lean supply[b]			Initial selectivity at oxygen-excess supply[b]		
Ethane oxidation		C_2H_4	CO	CO_2	C_2H_4	CO	CO_2
1.7	109.8	80.8	11.5	7.7	68.2	16.7	15.1
2.4	102.9	78.7	14.9	6.4	69.5	22.9	7.5
4.8	94.8	76.8	21.5	1.7	67.6	24.3	8.1
6.1	96.5	72.7	22.4	4.9	64.8	26.1	9.0
9.5	98.2	76.7	19.2	4.1	66.2	24.2	9.7
11.7	88.4	75.3	12.5	12.1	67.8	17.5	14.8
13.1	99.6	84.7	5.4	9.8	67.8	10.3	21.9
15.7	90.6	74.6	14.8	10.6	63.9	24.6	11.5
Ethylene oxidation		CH_3CHO	CO	CO_2	CH_3CHO	CO	CO_2
1.7	52.6	n.d.	78.2	21.8	n.d.	81.2	18.8
2.4	71.7	n.d.	82.0	18.0	n.d.	86.5	13.5
4.8	80.7	n.d.	91.0	9.0	n.d.	90.5	9.5
6.1	93.3	n.d.	88.3	11.7	n.d.	89.3	10.7
9.5	80.8	6.0	86.2	7.8	traces	93.3	6.7
11.7	70.2	6.1	88.8	5.1	4.8	93.4	1.7
13.1	88.8	54.3	31.3	14.4	36.2	49.8	14.0

[a] Data estimated from the rates of consumption of C_2H_6, C_2H_4, and CO, respectively.
[b] Data estimated from extrapolation of conversion–selectivity plots to zero conversion (based on data between 10 and 20% conversion). Herein the lower limit is given by the appearance of CO, for which the GC has a slightly lower sensitivity.

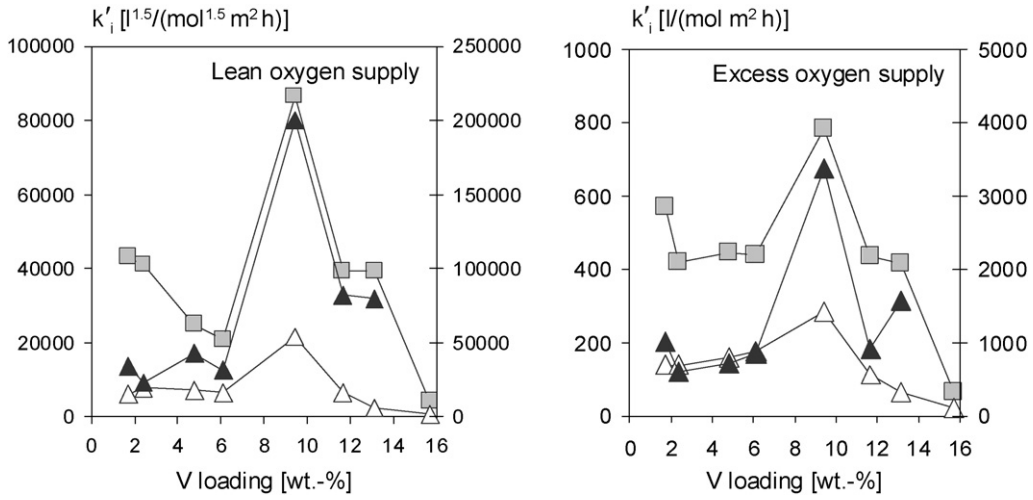

Fig. 10. Surface normalized turnover rate constants k_i' (see Eqs. (7) and (8)): (□) k_1', (△) k_2', and (▲) k_4'. Left-hand scales—reaction (1) (ethane to ethylene) and reaction (2) (ethane to CO). Right-hand scales—reaction (4) (ethylene to CO).

In principle, coke can be formed from ethylene and CO by pyrolysis and Boudouard reactions, respectively. We found that these reactions occur only if oxygen is consumed completely and at contact times much longer than those applied in this study. In this case, propylene, benzene, and toluene also can be formed from ethylene [40].

To establish relations between structure and activity, a reference temperature of 600 °C was chosen, comparable to the conditions in the TPR experiments reported in Section 3.2.3. Here all catalysts have adequate activity, which is sufficient to allow an accurate quantitative analysis of the product distribution. Based on standard estimations of the degree of pore utilization, diffusion limitations were found to be still negligible. They become significant at 630 °C, the highest temperature applied in the catalytic tests. At 600 °C, for oxygen-lean conditions, oxygen was almost completely consumed in the 4.8 and 6.1 wt% V samples and thus is the rate-limiting reactant. In all other experiments, the conversion was not limited by oxygen availability. Catalyst performance was analyzed taking into account the following network of six reactions:

$$C_2H_6 + 0.5O_2 \rightarrow C_2H_4 + H_2O, \quad (1)$$

$$C_2H_6 + 2.5O_2 \rightarrow 2CO + 3H_2O, \quad (2)$$

$$C_2H_6 + 3.5O_2 \rightarrow 2CO_2 + 3H_2O, \quad (3)$$

$$C_2H_4 + 2O_2 \rightarrow 2CO + 2H_2O, \quad (4)$$

$$C_2H_4 + 3O_2 \rightarrow 2CO_2 + 2H_2O, \quad (5)$$

$$CO + O_2 \rightarrow CO_2. \quad (6)$$

The rates of the partial reactions in the network were calculated from the initial product distribution and data on the oxidation of ethylene and CO. Because of the lack of acetaldehyde formation in ethane oxidation, its formation from ethylene and oxidation to CO, as well as the direct ethylene oxidation to CO, were put together in reaction (4). To evaluate correlations between the V species present on the catalysts and the catalyst performance, turnover rate constants at 600 °C were calculated for the reactions of the network, assuming reaction orders of 1 for ethane, ethylene, and carbon monoxide and 1/2 and 0 for oxygen in the lean mixture and under oxygen-excess conditions, respectively. The six turnover rate constants (k_1–k_6) were normalized to the available surface area of the catalysts (k_i') as follows:

$$k_i' = \frac{k_i}{m_{cat} \cdot S_{BET}} \quad \text{for } i = 1, \ldots, 6, \quad (7)$$

with

$$k_i = \frac{r_i}{\bar{c}_j \cdot \bar{c}_{O_2}^{0.5}} \quad \text{for oxygen-lean conditions}$$

and

$$k_i = \frac{r_i}{\bar{c}_j} \quad \text{for oxygen-excess conditions,}$$

where k_i' is the surface normalized turnover rate constant [$l^{1.5}/(mol^{1.5}\, m^2\, h)$ or $l/(mol\, m^2\, h)$], k_i is the turnover rate constant [$l^{1.5}/(mol^{1.5}\, h)$ or $l/(mol\, h)$], r_i is the turnover rate [mol reactant j/(mol V h)] at 600 °C, m_{cat} is the mass of the catalyst inserted into the reactor (g), S_{BET} is the BET specific surface area of the catalyst (m^2/g), $\bar{c}_j$ is the average concentration of reactant j (C_2H_6, C_2H_4, CO) (mol/L), and $\bar{c}_{O_2}$ is the average concentration of oxygen (mol/L).

The following discussion is focused on reactions (1), (2), and (4) as the main reactions determining catalytic performance. Reaction (1), the initial formation of ethylene from ethane, is known to occur via a Mars–van Krevelen mechanism under participation of reducible sites of the catalyst. Fig. 10 plots the surface area-normalized turnover rate constants k_i' ($i = 1, 2, 4$) for all catalysts versus V loading. To better understand this figure and Fig. 11, keep in mind that the turnover rate constants were calculated in a different manner for oxygen-lean and oxygen-excess conditions [see Eq. (7)] and cannot be compared directly. For the vanadate catalysts, a continuous decrease of k_1' with increasing V loading is observed up to 6.1 wt% V under oxygen-lean conditions, in contrast to oxygen-excess conditions, under which k_1' remains rather constant (except for the 1.7 wt% V-containing catalyst). The decrease in turnover

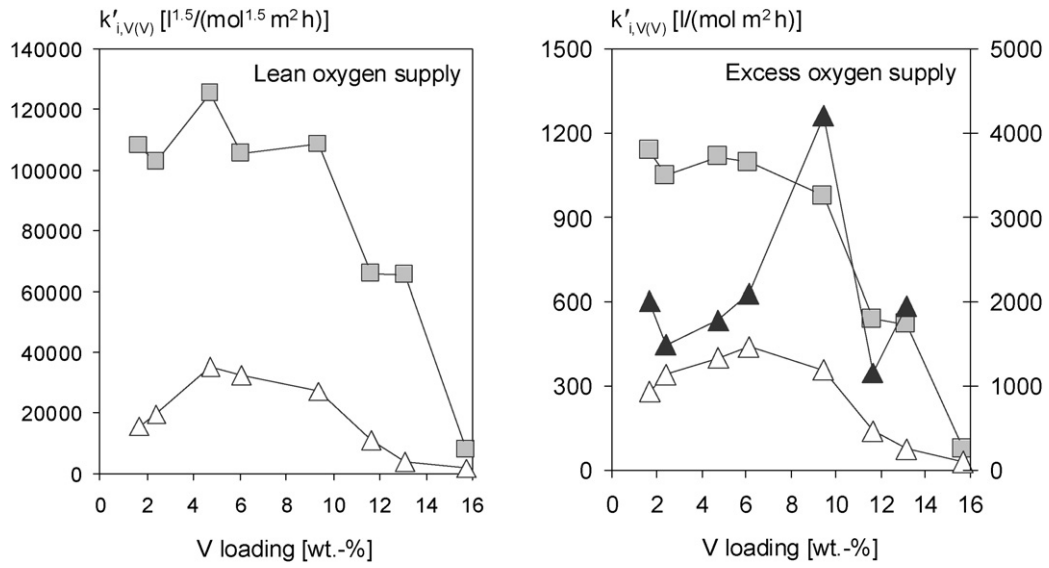

Fig. 11. Turnover rate constants k'_i (see Eqs. (7) and (8)) normalized to the surface area and the available V(V) fraction: (□) $k'_{1,V(V)}$, (△) $k'_{2,V(V)}$, and (▲) $k'_{4,V(V)}$. Left-hand scales—reaction (1) (ethane to ethylene) and reaction (2) (ethane to CO). Right-hand scale—reaction (4) (ethylene to CO).

rate constants under oxygen-lean conditions can be attributed to the limited availability of oxygen. In terms of V density, this tendency is similar to that reported in [19,21]. Under oxygen-excess conditions, the constancy of k'_1 is in agreement with the linear increase of the V density (see Table 1), which corresponds to a linear increase in the number of active sites and a similar reducibility of these sites.

In contrast to k'_1, k'_2 increases slightly with V loading. An even stronger tendency can be observed for k'_4.

Surprisingly, apart from the sample doped with 15.7 wt% V, the catalysts containing a V_2O_5 phase show equal or even higher normalized turnover rate constants than the vanadate-containing samples for all reactions. At first glance and with respect to reaction (1) (i.e., the formation of ethylene from ethane), this result seems to contradict the literature, which postulates the opposite order with respect to the performance of vanadates and V_2O_5 phases [5–7]. However, the TPR and XPS results reported above should be taken into account. According to the latter, only ∼33% of the V atoms are in the oxidation state V(V) in the vanadate catalysts, but nearly 80% of the V atoms are in the oxidation state V(V) in the catalysts containing a V_2O_5 phase, with the remainder being V(IV) in both catalysts. To prove the participation of only one of the different V species in the above reactions, the turnover rate constants were normalized to the vanadium oxidation state fractions [V(IV) or V(V)] (which were calculated from the TPR and XPS experiments, see Section 3.4) according to

$$k'_{i,V(n)} = k'_i / f, \tag{8}$$

where $k'_{i,V(n)}$ is the surface normalized turnover rate constant for the considered vanadium fraction ($l^{1.5}/(mol^{1.5}\,m^2\,h)$ or $l/(mol\,m^2\,h)$) and f is the fraction of V atoms in the respective oxidation state.

Meaningful results were obtained only when the V(V) fraction was considered active (see Fig. 11). For ethylene formation from ethane (reaction (1)), the catalysts with V loadings up to 9.5 wt% have a similar V(V)-specific activity independent on surface area and percentage of V(V) in the present working state for both lean and oxygen-excess conditions. This correlates with the identical reducibility of these catalysts after time on stream pretreatment (Fig. 7). The decrease in the V(V) specific activity observed here for the catalysts loaded with 11.7–15.7 wt% V is consistent with the nonaccessibility of the deeper layers of the V_2O_5 crystallites detected in the corresponding TPR patterns (Fig. 7). Catalyst reduction, which was measured in cases of complete oxygen consumption and hydrocarbon excess as it was found for the 4.8 and 6.1 wt% V catalysts, results in a loss of activity in ethylene formation due to the disappearance of the V(V) species. Apparently, the V(IV) fraction, which is reducible by hydrogen, is not able to activate ethane.

As can be seen from Fig. 11, the CO formation from ethane (reaction (2)) increases initially with the degree of vanadate polymerization, but returns to the level of isolated vanadates when V_2O_5 crystallites appear. This tendency is opposite to that of Brønstedt acidity, which was found to be lower for polyvanadate than for isolated vanadate species and V_2O_5 crystallites. Based on our findings and on the literature data (e.g. [5,20,98–104]), it is sensible to correlate primary CO formation to the number and strength of Brønstedt acid sites. Again, the correlation of activity to V(V) is stronger than that to V(IV) or to the total vanadia content. In agreement with Le Bars et al. [21], we found that Lewis acidity plays only a minor role in catalyst performance. Finally, the consecutive ethylene oxidation to CO appears to be favored by the presence of bulk-like V_2O_5 crystallites.

It should be noted that all results regarding reducibility, oxidation states, acid–base properties, phase transformations, and catalytic activity reported herein could be fully reproduced in experiments with another series of VO_x catalysts prepared by impregnation of γ-alumina with NH_4VO_3 in water–acetone mixtures and subsequent calcination at 650 °C. The sole impact of preparation procedure was a somewhat lower dispersion of

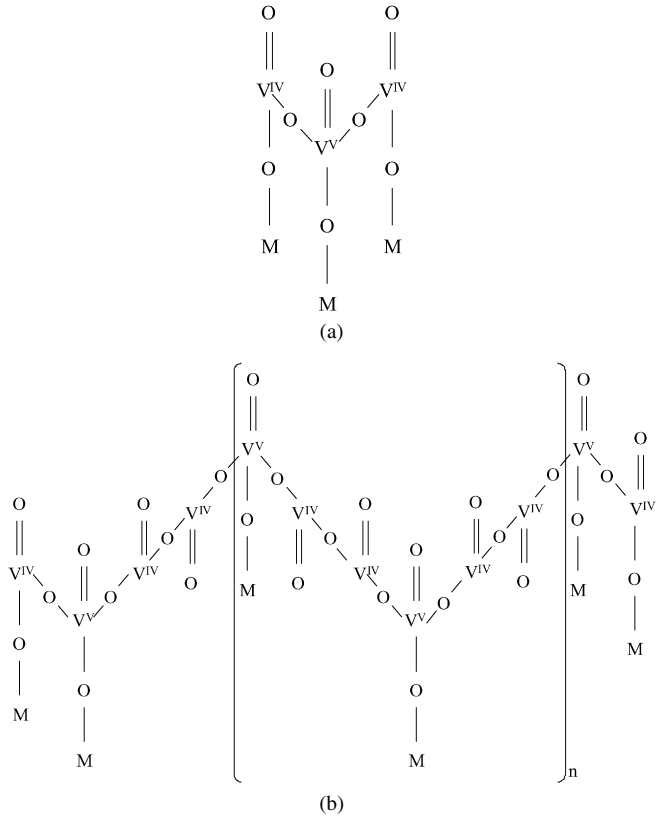

Fig. 12. Proposed vanadate species: (a) isolated amorphous vanadate ($[V_3O_8]^{3-}$ base unit); (b) 'polyvanadate' chain structure.

vanadia, leading to XRD detection of V_2O_5 already at a loading of 5.5 wt%. These results are consistent with data reported in [19,21].

3.6. Proposed structure of VO_x/γ-Al_2O_3 catalysts

The coexistence of two kinds of vanadium atoms with different redox behavior within the vanadate structure can be reflected in a new structural model that is in agreement with our findings as well as previous reports. The high sensitivity of the catalytic performance on the kind of support suggests an assignment of the active V(V) species to the M–O–V bond as the crucial site for performance, reducibility, and acid–base properties. On the other hand, TPR and XPS results reveal that in the dispersed vanadate catalysts only $\sim 1/3$ of the V atoms are in this oxidation state and $\sim 2/3$ occupy the oxidation state $+4$.

The smallest structural unit that can fulfill these requirements is $[V_3O_8]^{3-}$ (see Fig. 12a), with three bonds to the support and a V(V)/V(IV) ratio of 1:2, as found in the experiments. We suggest that this structure is present predominantly in low-loaded catalysts (<2 V atoms/nm^2), where the vanadia phase was found to be amorphous and described as "isolated vanadates." However, for ultra-low loadings, the existence of other structures [e.g., the up-to-now favored $(VO_4)^{3-}$ monovanadate unit], cannot not be ruled out completely.

At loadings above 2 V atoms/nm^2 but below the appearance of V_2O_5, a polymerized vanadate phase appears that differs from the isolated vanadates by a long-range ordered structure and lower Brønstedt acidity, resulting in a different initial product distribution. XPS and TPR findings suggest a similar ratio of V(V)/V(IV) as above. In addition, comparable behavior with respect to reducibility and initial ethylene formation is observed. The "polyvanadate" net structure proposed in Fig. 12b consists of chains with $[V_3O_7]^-$ as the base unit and reproduces the experimentally observed ratio of oxidation states. Note that except for comparable reducibility, this polyvanadate structure differs from the amorphous V(V) overlayer phase formed from V_2O_5 crystallites during exposure to oxygen–ethane mixtures.

The two vanadate structures are stable against redox cycles in hydrocarbon oxidation, but they might collapse if vanadia is reduced (by, e.g., hydrogen) to V(III). Note that V(IV)–V(V) mixed oxides, like V_6O_{13}, are also known to exist for bulk species [12,105].

It is important to note that the proposed structures are in agreement with previous spectroscopic findings on vanadate catalysts. V=O, M–O–V, and V–O–V bonds (which cause, e.g., the various known IR and Raman absorptions) are included, and not in contradiction to the average oxidation state experimentally found in the study reported herein.

4. Conclusions

In the present study, γ-alumina-supported vanadia catalysts with loadings of 1.7–15.7 wt% were investigated to evaluate structural properties, redox cycles, and changes due to exposure to various reactive environments. Three different vanadia phases were identified for fresh catalysts: amorphous isolated vanadate species (<2 atoms V/nm^2), well-ordered polyvanadate species (2–5 V atoms/nm^2), and bulk-like V_2O_5 crystallites. The two vanadate phases showed identical reducibility, but different Brønstedt acidity. The bulk-like V_2O_5 crystallites, in turn, were less reducible; their acidity was similar to that of isolated vanadate and thus greater than that of polyvanadates.

Structural changes were observed on exposure of the catalysts to various redox environments. H_2-TPR–O_2-TPO sequences lead to a more reducible species from isolated vanadates, whereas polyvanadate and crystalline V_2O_5 phases remain almost unaffected. In contrast, under time on stream in ethane oxidation, neither vanadate phase was modified, but a new phase was formed from the V_2O_5 crystallites with a reducibility similar to that of the vanadates. This phase transformation can even be complete. It seems that such phase conversions are specific to the reactive environment and also are reversible if any changes occur in the reactant system to which the catalyst is exposed.

A comparison of TPR and XPS data shows that even under oxidizing conditions in vanadate catalysts, only $\sim$30% of V is in the oxidation state $+5$, whereas the majority is present as V(IV). In V_2O_5 phases, the V(V) fraction is much larger, typically 80% even after phase transformation by exposure to hydrocarbon oxidation (if oxygen is not limiting). In both cases, reduction by hydrogen in TPR leads to a final oxidation state of $+3$.

These results contradict the common assumption that V(V) is the only oxidation state in oxidized vanadia catalysts, par-

ticularly for those containing well-dispersed vanadate species. Consequently, the presence of two different kinds of V species within the vanadates on γ-alumina with different redox cycles, V(IV) $\leftrightarrow$ V(III) and V(V) $\leftrightarrow$ V(III), can be concluded. The maximum V(V) fraction of $\sim$30% for the vanadate phases is independent of V loading and indicates that both V(IV) and V(V) are well distributed within the vanadate layer; a "core–shell" structure seems unlikely. We suggest that the smallest unit present in the amorphous vanadate phase comprises one V(V) cation and two V(IV) cations bridged and bound to the γ-alumina support via oxygen, resulting in the composition $[V_3O_8]^{3-}$. We postulate chains consisting of $[V_3O_7]^{-}$ units for the well-ordered polyvanadates.

These suggestions are supported by experiments on the selective oxidation of ethane as well as analyses of structure–activity relationships. TPR and XPS measurements confirmed that V(V) is the necessary species for the activation of ethane and V(IV) is not involved. The TPR experiments with different ethane–oxygen mixtures indicate that in ethane oxidation under steady-state conditions, the catalysts are in the oxidized state, independent of the nature of the active vanadia phase, because reoxidation is faster than hydrocarbon activation. Significant catalyst reduction and loss of activity occurs only if the surrounding gas-phase oxygen is completely consumed. This aspect should be considered in the design of reactors operated under oxygen-shortage conditions, such as membrane reactors or periodically operated fixed-bed reactors.

Our surface-sensitive experiments and the independent catalytic tests have revealed the existence of distinct V species in the studied γ-alumina-supported vanadia catalysts. The role and possible structure of the detected V species should be taken into account in future investigations of vanadia phases in supported catalysts.

Acknowledgments

Financial support was provided by the Deutsche Forschungsgemeinschaft (research unit 447, "Membrane-Supported Reaction Engineering"). The authors thank Dr. R. Wagner (Otto von Guericke University, Magdeburg) for assistance with the DRIFTS measurements, and N. Pfänder, Dr. D. Su, and G. Weinberg (Fritz-Haber Institute, Berlin) for the TEM images.

References

[1] K. Hodnett, Heterogeneous Catalytic Oxidation: Fundamental and Technological Aspects of the Selective and Total Oxidation of Organic Compounds, Wiley, New York, 2000.
[2] K. Weissermel, H.-J. Arpe, Industrial Organic Chemistry, vol. 3, completely rev. ed., VCH, Weinheim, 1997.
[3] F. Cavani, F. Trifiro, Catal. Today 51 (1999) 561–580.
[4] J.N. Armor, Appl. Catal. A Gen. 222 (2001) 407–426.
[5] M.A. Banares, Catal. Today 51 (1999) 319–348.
[6] C.L. Pieck, M.A. Banares, J.L.G. Fierro, J. Catal. 224 (2004) 1–7.
[7] Y.-M. Liu, Y. Cao, N. Yi, W.-L. Feng, W.-L. Dai, S.-R. Yan, H.-Y. He, K.-N. Fan, J. Catal. 224 (2004) 417–428.
[8] X. Gao, M.A. Banares, I.E. Wachs, J. Catal. 188 (1999) 325–331.
[9] M.L. Ferreira, M. Volpe, J. Mol. Catal. 184 (2002) 349–360.
[10] G. Deo, I.E. Wachs, J. Haber, Crit. Rev. Surf. Chem. 4 (1994) 141–187.
[11] E.A. Mamedow, V. Cortés Corberán, Appl. Catal. A 127 (1995) (1994) 1–40.
[12] J. Haber, M. Witko, R. Tokarz, Appl. Catal. A 157 (1999) (1994) 3–22.
[13] B. Grzybowska-Swierkosz, Appl. Catal. A 157 (1999) (1994) 409–420.
[14] B.M. Weckhuysen, D.E. Keller, Catal. Today 78 (2003) 25–46.
[15] E. García-Bordejé, J. Lázaro, R. Moliner, J.F. Galindo, J. Sotres, A.M. Baro, Appl. Surf. Sci. 228 (2004) (1994) 135–142.
[16] G. Centi, Appl. Catal. A Gen. 147 (1996) 267–298.
[17] I.E. Wachs, B.M. Weckhuysen, Appl. Catal. A Gen. 157 (1997) 67–90.
[18] A. Khodakov, J. Yang, S. Su, E. Iglesia, A.T. Bell, J. Catal. 177 (1998) 343–351.
[19] M.D. Argyle, K. Chen, A.T. Bell, E. Iglesia, J. Catal. 208 (2002) 139–149.
[20] T. Blasco, J.M.L. Nieto, Appl. Catal. A 157 (1997) 117–142.
[21] J. Le Bars, A. Auroux, M. Forissier, J.C. Vedrine, J. Catal. 162 (1996) 250–259.
[22] O.L.J. Gijzeman, J.N.J. van Lingen, J.H. van Lenthe, S.J. Tinnemans, D.E. Keller, B.M. Weckhuysen, Chem. Phys. Lett. 397 (2004) 277–281.
[23] D.E. Keller, F.M.F. de Groot, D.C. Konigsberger, B.M. Weckhuysen, J. Phys. Chem. B 109 (2005) 10223–10233.
[24] M. Abu Haija, S. Guimond, Y. Romanyshyn, A. Uhl, H. Kuhlenbeck, T.K. Todorova, M.V. Ganduglia-Pirovano, J. Döbler, J. Sauer, H.-J. Freund, Surf. Sci. 600 (2006) 1497–1503.
[25] J. Keränen, A. Auroux, S. Ek, L. Niinistö, Appl. Catal. A 228 (2002) 213–225.
[26] I.E. Wachs, Y. Chen, J.-M. Jehng, L.E. Briand, T. Tanaka, Catal. Today 78 (2003) 13–24.
[27] J.M. Kanervo, M. Elina Harlin, A.O.I. Krause, M.A. Banares, Catal. Today 78 (2003) 171–180.
[28] P. Concepción, M.T. Navarro, T. Blasco, J.M. López Nieto, B. Panzacchi, F. Rey, Catal. Today 96 (2004) 179–186.
[29] K.V.R. Chary, G. Kishan, C.P. Kumar, G.V. Sagar, Appl. Catal. A 246 (2003) 335–350.
[30] M.M. Koranne, J.G. Goodwin Jr., G. Marcelin, J. Catal. 148 (1994) 369–377.
[31] H.K. Matralis, M. Ciardelli, M. Ruwet, P. Grange, J. Catal. 157 (1995) 368–379.
[32] D.I. Enache, E. Bordes-Richard, A. Ensuque, F. Bozon-Verduraz, Appl. Catal. A Gen. 278 (2004) 93–102.
[33] E.P. Reddy, R.S. Varma, J. Catal. 221 (2004) 93–104.
[34] B.M. Reddy, I. Ganesh, A. Khan, J. Mol. Catal. A Chem. 223 (2004) 295–304.
[35] S. Djerad, L. Tifouti, M. Crocoll, W. Weisweiler, J. Mol. Catal. A Chem. 208 (2004) 257–264.
[36] J.B. Stelzer, A. Feldhoff, J. Caro, M. Fait, D. Habel, E. Feike, H. Schubert, Chem. Ing. Technol. 76/8 (2004) 1086–1092.
[37] Casa Software Ltd., United Kingdom; http://www.casaxps.com/.
[38] F. Klose, T. Wolff, S. Thomas, A. Seidel-Morgenstern, Catal. Today 82 (2003) 25–40.
[39] F. Klose, T. Wolff, S. Thomas, A. Seidel-Morgenstern, Appl. Catal. A Gen. 257 (2004) 193–199.
[40] F. Klose, M. Joshi, C. Hamel, A. Seidel-Morgenstern, Appl. Catal. A Gen. 260 (2004) 101–110.
[41] Powder diffraction database PDF-2 (Set 53, Release 2003), International Centre for Diffraction Data, Newton Square PA, 2003.
[42] N. Magg, J.B. Giorgi, T. Schroeder, M. Bäumer, H.-J. Freund, J. Phys. Chem. B 106 (2002) 8756–8761.
[43] N. Magg, B. Immaraporn, J.B. Giorgi, T. Schroeder, M. Bäumer, J. Döbler, Z. Wu, E. Kondratenko, M. Cherian, M. Baerns, P.C. Stair, J. Sauer, H.-J. Freund, J. Catal. 226 (2004) 88–100.
[44] M. Panizza, C. Resini, F. Raccoli, G. Busca, R. Catani, St. Rossini, Chem. Eng. J. 93 (2003) 181–189.
[45] J. Le Bars, J.C. Védrine, A. Auroux, S. Trautmann, M. Baerns, Appl. Catal. A 119 (1994) 341–354.
[46] Z. Wu, H.S. Kim, P.C. Stair, S. Rugmini, S.D. Jackson, J. Phys. Chem. B 109 (2005) 2793–2800.
[47] T. Blasco, A. Galli, J.M. López Nieto, F. Trifiró, J. Catal. 169 (1997) 203–211.

[48] S. Lim, G. Haller, Appl. Catal. A Gen. 188 (1999) 277–286.
[49] G. Busca, Langmuir 2 (1986) 577–582.
[50] T.J. Dines, C.H. Rochester, A.M. Ward, J. Chem. Faraday Trans. 87 (1991) 1611–1616.
[51] L. Kiwi-Minsker, D.A. Bulushev, F. Rainone, A. Renken, J. Mol. Catal. Chem. 184 (2002) 223–235.
[52] G. Busca, Phys. Chem. Chem. Phys. 1 (1999) 723–736.
[53] N. Pfänder, D. Su, G. Weinberg, Fritz-Haber-Institut der Max-Planck-Gesellschaft, Berlin, Germany.
[54] A. Gervasini, P. Carniti, J. Keränen, L. Niinistö, A. Auroux, Catal. Today 96 (2004) 187–194.
[55] C. Téllez, M. Abon, J.A. Dalmon, C. Mirodatos, J. Santamaria, J. Catal. 195 (2000) 113–124.
[56] S. Besselmann, C. Freitag, O. Hinrichsen, M. Muhler, Phys. Chem. Chem. Phys. 3 (2001) 4633–4638.
[57] A.W. Stobbe-Kreemers, G.C. van Leerdam, J.P. Jacobs, H.H. Brongersma, J.J.F. Scholten, J. Catal. 152 (1995) 130–136.
[58] M.L. Ferreira, M. Volpe, J. Mol. Catal. 184 (2002) 349–360.
[59] E.P. Reddy, R.S. Varma, J. Catal. 221 (2004) 93–104.
[60] J.M. Kanervo, M.E. Harlin, A.O.I. Krause, M.A. Banares, Catal. Today 78 (2003) 171–180.
[61] T.K. Todorova, M.V. Ganduglia-Pirovano, J. Sauer, J. Phys. Chem. B 109 (2005) 23523–23532.
[62] V. Brázdová, M.V. Ganduglia-Pirovano, J. Sauer, J. Phys. Chem. B 109 (2005) 23532–23542.
[63] I.E. Wachs, Y. Chen, J.M. Jehng, L.E. Briand, T. Tanaka, Catal. Today 78 (2003) 13–24.
[64] N. Ballarini, F. Cavani, A. Cericola, C. Cortelli, M. Ferrari, F. Tifirò, G. Capannelli, A. Comite, R. Catani, U. Cornaro, Catal. Today 91–92 (2004) 99–104.
[65] J. Le Bars, A. Auroux, M. Forissier, J.C. Vedrine, J. Catal. 162 (1996) 250–259.
[66] F. Arena, F. Frusteri, A. Parmaliana, Appl. Catal. A Gen. 176 (1999) 189–199.
[67] P. Mars, D.W. Krevelen, Chem. Eng. Sci. (Spec. Suppl.) 3 (1954) 41–59.
[68] J.H. McCain, US Patent 4,524,236 (1985).
[69] J.M. López Nieto, P. Botella, M.I. Vázquez, A. Dejoz, WO patent 03/064035, 2003.
[70] P. Botella, E. García-González, A. Dejoz, J.M. López Nieto, M.I. Vázquez, J.M. González-Calbet, J. Catal. 225 (2004) 428–438.
[71] P. Botella, A. Dejoz, J.M. López Nieto, P. Concepción, M.I. Vázquez, Appl. Catal. A Gen. 298 (2006) 16–23.
[72] Mitsubishi Chem. Corp., EP 0608838A2 (1994).
[73] T. Ushikubo, H. Nakamura, Y. Koyasu, S. Wajiki, US Patent 5,380,933 (1995).
[74] E.K. Novakova, J.C. Védrine, E.G. Derouane, J. Catal. 211 (2002) 226–234.
[75] D. Vitry, Y. Morikawa, J.L. Dubois, W. Ueda, Appl. Catal. A Gen. 251 (2003) 411–424.
[76] J.N. Al-Saeedi, V.V. Guiliants, O. Guerro-Pérez, M.A. Banares, J. Catal. 215 (2003) 108–115.
[77] J.M. Oliver, J.M. López Nieto, P. Botella, Catal. Today 96 (2004) 241–249.
[78] E. Balcells, F. Borgmeier, I. Grißtede, H.G. Lintz, Catal. Lett. 87 (2003) 195–199.
[79] M. Hatano, A. Kayo, US Patent 5,049,692 (1991); M. Hatano, A. Kayo, EP 0,318,295B1 (1992).
[80] O. Guerro-Pérez, J.N. Al-Saeedi, V.V. Guiliants, M.A. Banares, Appl. Catal. A Gen. 260 (2004) 93–99.
[81] Z. Zhao, X. Gao, I.E. Wachs, J. Phys. Chem. B 107 (2003) 6333–6342.
[82] L.K. Rihko-Struckmann, Y. Ye, L. Chalakov, Y. Suchorski, H. Weiss, K. Sundmacher, Catal. Lett. 109 (2006) 89–96.
[83] M. Abon, K.E. Bere, A. Tuel, P. Delishere, J. Catal. 156 (1995) 28–36.
[84] P. Delishere, K.E. Bere, M. Abon, Appl. Catal. A Gen. 172 (1998) 295–309.
[85] S. Albonetti, F. Cavani, F. Trifiro, P. Venturoli, G. Calestani, M. Lopez-Cranados, J.L.G. Fierro, J. Catal. 160 (1996) 52–64.
[86] Y. Suchorski, B. Munder, S. Becker, L. Rihko-Struckmann, K. Sundmacher, H. Weiss, Appl. Surf. Sci. (2007), in press, doi:10.1016/j.apsusc.2006.12.082.
[87] Y. Suchorski, L. Rihko-Struckmann, F. Klose, Y. Ye, M. Alandjiyska, K. Sundmacher, H. Weiss, Appl. Surf. Sci. 249 (2005) 231–237.
[88] G.W. Coulston, E.A. Thompson, N. Herron, J. Catal. 163 (1996) 122–129.
[89] J. Haber, M. Witko, R. Tokarz, Appl. Catal. A Gen. 157 (1999) 3–22.
[90] M.P. Casaletto, L. Lisi, G. Mattogno, P. Patrono, G. Ruopollo, G. Russo, Appl. Catal. A 226 (2002) 41–48.
[91] S.T. Oyama, G.A. Somorjai, J. Phys. Chem. 94 (1990) 5022–5028.
[92] P. Concepción, M.T. Navarro, T. Blasco, J.M. López Nieto, B. Panzacchi, F. Rey, Catal. Today 96 (2004) 179–186.
[93] M.A. Banares, M.V. Martínez-Huerta, X. Gao, J.L.G. Fierro, I.E. Wachs, Catal. Today 61 (2000) 295–301.
[94] R. Grabowski, J. Sloczynski, Chem. Eng. Proc. 44 (2005) 1082–1093.
[95] E. Heracleous, A.A. Lemonidou, Catal. Today 112 (2006) 23–27.
[96] A. Bottino, G. Capannelli, A. Comite, S. Storace, R.D. Felice, Chem. Eng. J. 4142 (2003) 1–8.
[97] P.T. Wierzchowski, L.W. Zatorski, Appl. Catal. B Environ. 44 (2003) 53–65.
[98] P.M. Michalakos, M.C. Kung, I. Jahan, H.H. Kung, J. Catal. 140 (1993) 226–242.
[99] H.H. Kung, Adv. Catal. 40 (1994) 1–38.
[100] Z. Magagula, E. van Steen, Catal. Today 49 (1999) 155–160.
[101] G. Centi, Catal. Today 56 (2000) 443–453.
[102] B. Grzybowska-Swierkosz, Top. Catal. 21 (2002) 35–46.
[103] H.X. Dai, C.T. Au, Curr. Top. Catal. 3 (2002) 33–80.
[104] Z.S. Chao, E. Ruckenstein, Catal. Lett. 88 (2003) 147–154.
[105] I.E. Wachs, Y. Chen, J.-M. Jehng, L.E. Briand, T. Tanaka, Catal. Today 78 (2003) 13–24.